Chapter I

Spin dynamics in Mn-doped positively charged quantum dots

Magnetic anisotropy depends on the local environment of magnetic atoms, and are a crucial properties for modern storage devices. We saw in Sec. **??** that the Mn atom in neutral, self-assembled QD presents a small anisotropy of a few tens of μeV. It is expected that a Mn atom could develop a large anisotropy energy in the meV range when it is exchange coupled with a single confined heavy-hole spin [1]. The two low energy hole-Mn state behave like an Ising spin system, forming an atomic ferromagnet. In addition the exchange induced Mn spin magnetic anisotropy could be electrically controlled by changing the Mn/hh overlap with a bias voltage applied across the QD.

In this chapter, we look at the spin dynamics of a Mn spin coupled to a single hole in a CdTe/ZnTe QD. We begin presenting the energy structure of this system. We show that Λ-level systems are formed between the hybrid spin states formed by the hole-Mn system in the ground state, and the electron-Mn states in the excited state. Those systems can be addressed independently with a resonant laser and are used to study the dynamics of the hole-Mn hybrid spin.

In the second section, we study the dynamics of the h-Mn hybrid spin through two experiments: auto-correlation of the resonant PL and resonant optical pumping experiments. We identified an efficient relaxation channel for this hybrid spin via the interplay of the exchange interaction between the hole and the magnetic atom, as well as the coupling to accoustic phonons. We also show that the optical Λ-systems are connected through inefficient spin-flips that can be enhanced under weak transverse magnetic field. The dynamics of the resonant PL of a p-doped magnetic QD is well described by a complete rate equation model.

In the last section, we look at the electron-Mn coherent dynamics, directly observed in the time resonant PL. Quantum beats reflecting the coherent transfer of population between e-Mn spin states, mixed by an anisotropic strain in the plane

of the quantum dot, are clearly observed. We highlight that this strain induced coherent coupling is tunable with an external magnetic field.

I.1 Mn in a positively charged CdTe quantum dot

I.1.1 Spin structure of a positively charged Mn doped quantum dot

We saw in Sec. ?? that the exchange interaction between the hole and the Mn spin lifts the degeneracy of the Mn spin states. The recombination of the exciton states are then each split into six lines. For a given polarization, each line corresponds to a given Mn spin state. The ground state of a Mn-doped positively charged quantum dot is formed by a single hole coupled to the Mn atom, leading to the same kind of splitting. Via the application of a positive bias voltage (V > 0) on the sample with a Schottky gate (see Sec. ??), a single hole is trapped in the magnetic QD and the emission of the positively charged exciton becomes largely dominant (Fig. I.1 (a)). The PL of such a QD is presented in Fig. I.1 (b).

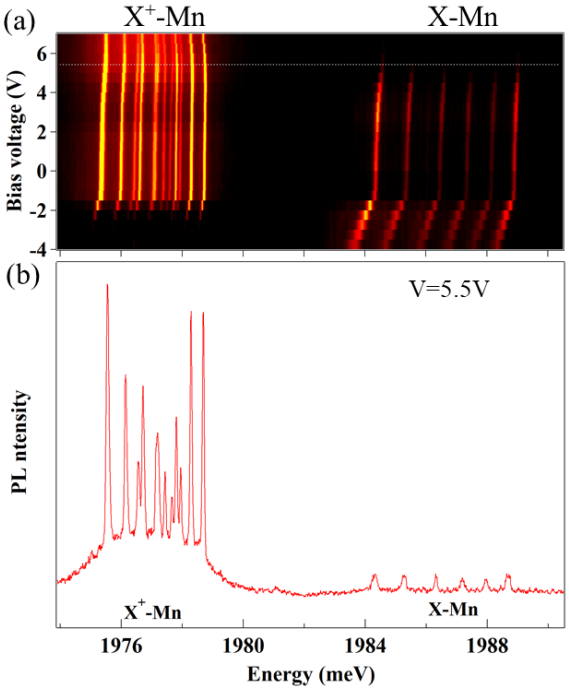

Figure I.1: (a) Color scale plot of the PL intensity of one QD of sample M3085, embedding a single Mn inserted in Schottky structure, showing the emission of the neutral (X-Mn) and positively charged (X^+-Mn) exciton as a function of energy and bias voltage. (b) Cut in the map shown in (a) fo V = 5.5 V

As discussed in Sec. ??, in a strained self-assembled CdTe QD, a Mn atom exhibits a fine structure dominated by a weak magnetic anisotropy. Neglecting

the tetrahedral crystal field of the CdTe matrix, this fine structure is described by the effective spin Hamiltonian:

$$\mathcal{H}_{Mn,CF} = D_0 S_z^2 + E(S_x^2 - S_y^2) \tag{I.1}$$

with D_0 depicting the effect of the biaxial strain and E describing a possible anisotropy of the strain in the plane of the QD. It was shown that an anisotropy of strain in the 1 μeV range was essential to understand the absence of pumping for Mn in strain-free quantum dots [2] and is thus included here to remain general. We will study more in details the effect of the coupling term E in Sec. I.2.

When a hole is trapped in a QD containing a single Mn, the spin structure is controlled by the hole-Mn exchange interaction that reads:

$$\mathcal{H}_{hMn}^{ex} = I_{hMn} \mathbf{S} \cdot \mathbf{J} \tag{I.2}$$

with I_{hMn} the exchange energy between the hole and the Mn and $\mathbf{J}$ the hole spin operator. In the presence of heavy-hole/light-hole mixing, $\mathbf{J}$, represented in the basis of the two low energy heavy-hole states, is related to the Pauli matrices by $J_z = 3/2\tau_z$ and $J_\pm = \xi\tau_\pm$ with $\xi = -2\sqrt{3}e^{-2i\theta}\rho_c/\Delta_{lh}$, $\tau_+ = \tau_x + i\tau_y$ and $\tau_- = \tau_x - i\tau_y$, τ_x, τ_y, τ_z being the Pauli matrices. ρ_c is the coupling energy between heavy holes and light holes separated by an effective energy splitting Δ_{lh}. θ is the angle relative to the [110] axis of the principal axis of the anisotropy (shape and/or strain) responsible for the heavy-hole/light-hole mixing [3, 4]. The matrices J_z and $J_\pm$ are described with more details in Eq. **??** to **??**. For a weak valence band mixing, the hole-Mn energy levels are mainly controlled by $I_{hMn}S_zJ_z$ and form 12 eigenstates organized in 6 doublets with well-defined S_z and J_z. These states are labelled $|S_z, J_z\rangle$.

when an e-h pair is optically created, a positively charged exciton X^+ forms with the hole trapped in the QD via the bias voltage, coupled with the Mn atom. The two holes associate with anti-parallel spins. Thus, in the excited state, the system is dominated by the electron-Mn exchange interaction:

$$\mathcal{H}_{eMn}^{ex} = I_{eMn} \mathbf{S}.\boldsymbol{\sigma} \tag{I.3}$$

with, as usual, $\boldsymbol{\sigma}$ the electron spin and I_{eMn} the e-Mn exchange energy. This interaction is isotrope, and results in a ground state septuplet of total spin $M = 3$ and a fivefold degenerated manifold of total spin $M = 2$, for a total of twelve electron-Mn states. In the absence of perturbations, the energy levels of each of those manifold are degenerated. Each of those states are labelled $|M, M_z\rangle$. They are presented in Fig. I.2, as well as the resulting recombination from each of the manifold. One can see that the photon emission from each excited states occurs at a given energy, resulting in twelve possible PL peaks.

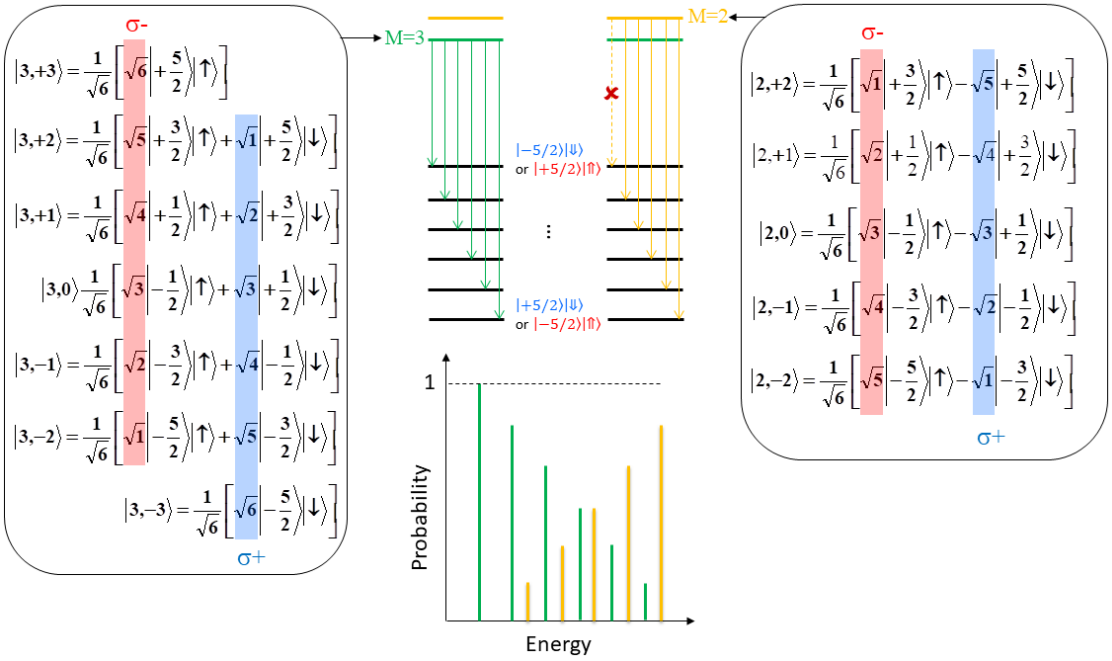

Figure I.2: Electron-Mn spin and hole-Mn energy levels. For each e-Mn state $|M, M_z\rangle$, we highlighted the weight of each recombination path in a given polarization ($\sigma-$ (red) and $\sigma+$ (blue)). This weight is directly linked to the intensity of each peak. In the center, the different possible recombination paths for $M = 3$ and $M = 2$ are illustrated, with a schema of the resulting spectra below.

As shown in Fig. I.2, in a given polarization, we can associate a transition from an excited state to a single ground state. As discussed in Sec. **??**, the polarization of the transition is given by the spins of the carriers that recombines, without affecting the Mn spin, as shown in Sec. **??**. We then see that all level associated with the $M = 2$ quintuplet can recombine in both polarizations, while only 6 level of the $M = 3$ septuplet can recombine in a given polarization. This leads to 11 spectrally resolved lines. Each of these lines can be associated to a single e-Mn state.

To illustrate this association, let's consider the recombinations in $\sigma+$ polarization, meaning we consider the annihilation of the e-h pair $|\downarrow_e, \Uparrow_h\rangle$. We have an excited state of the form $|M, M_z\rangle = \alpha|S_z, \downarrow_e\rangle + \beta|S_z - 1/2, \uparrow_e\rangle$ and a final state after the e-h annihilation $|S_z, \Downarrow_h\rangle$, which is an eigenstate of the hamiltonian $\mathcal{H}_{h-Mn}$. The intensity of the optical transition is given by the overlap $\langle M, M_z|S_z, \downarrow_e\rangle$, which is the Clebsh-Gordan coefficient appearing in the composition of a spin $1/2$ with a spin $5/2$, here noted α for the initial state associated with the $\sigma+$ transition. Let's

focus on the transition linked with the high energy final state $|-5/2, \Downarrow_h\rangle$. In order to have this state as a final state, the initial state has to be $|\Uparrow_h, \Downarrow_h\rangle \times |-5/2, \downarrow_e\rangle$. Only the excited state $|3,-3\rangle$ have this e-Mn state, this transition being forbidden from the $M = 2$ quintuplet. Since $|3,-3\rangle$ is a pure e-Mn state, this transition has the highest optical transition weight.

We can repeat this operation with each h-Mn state, in both polarizations. They can all be associated with both $|2, M_z\rangle$ and $|3, M_z\rangle$ initial states, with optical weights lying between 1/6 and 5/6. The only exception is the other high energy final state, $|+5/2, \Uparrow_h\rangle$, only associated with the initial state $|3,+3\rangle$ in $\sigma-$ polarization. For a given polarization, we then have 11 resolved lines. The resulting PL for the X^+-Mn is illustrating at the bottom of Fig. I.2 and can be seen as a superposition of two structures: six lines which intensities decrease with increasing their energy position (transitions from $M = 3$ states) and fives lines which intensities increase with increasing their energy position (transitions from $M = 2$ states).

There are two things we neglected in the previous paragraphs: the Valence Band Mixing and the perturbative effect of the hole-Mn exchange interaction. The VBM mixes the h-Mn states two by two, and induces population transfer between the different levels [5]. For $\rho_s/\Delta_{lh} \ll 1$, the effect of this interaction is small both on the wave function and on the degeneracy of all the h-Mn doublets except the third, which is split. This is illustrated in Fig. I.3 (a) by the two split doted levels. These states are the bonding and antibonding combinations of $|S_z = -1/2, \Uparrow_h\rangle$ and $|S_z = +1/2, \Downarrow_h\rangle$. They are coupled via linearly polarized photons to the $|2, 0\rangle$ and $|3, 0\rangle$ e-Mn states, giving the four linearly polarized lines observed on Fig. I.3 (b).

The wave function of the hole in the ground state and of the charged exciton in the excited state are also perturbed by the h-Mn exchange interaction. This perturbation depends on the value of the exchange energy between the Mn spin S_z and the hole spin J_z. It can be represented using second-order perturbation theory by an effective spin hamiltonian [6–8]:

$$\mathcal{H}_{scat} = -\eta S_z^2 \tag{I.4}$$

with $\eta > 0$. This perturbation has to be taken into account twice in the excited state where there are two holes interacting with the Mn. It is responsible for the irregular energy spacing of the X^+-Mn spectra, that can be seen on Fig. I.1 (b) and I.3 (b).

Including the effect of a magnetic field $\mathbf{B}$, we can write hamiltonian of the ground state (h-Mn):

$$\begin{aligned} \mathcal{H}_{hMn} = &\ \mathcal{H}^{ex}_{hMn} + \mathcal{H}_{scat} + \mathcal{H}_{CF,Mn} + \mathcal{H}_{mag,GS} \\ = &\ I_{hMn}\mathbf{S}.\mathbf{J} - \eta S_z^2 + D_0 S_z^2 + E(S_x^2 - S_y^2) + g_{Mn}\mu_B \mathbf{S}.\mathbf{B} + g_e \mu_B \mathbf{J}.\mathbf{B} \end{aligned} \tag{I.5}$$

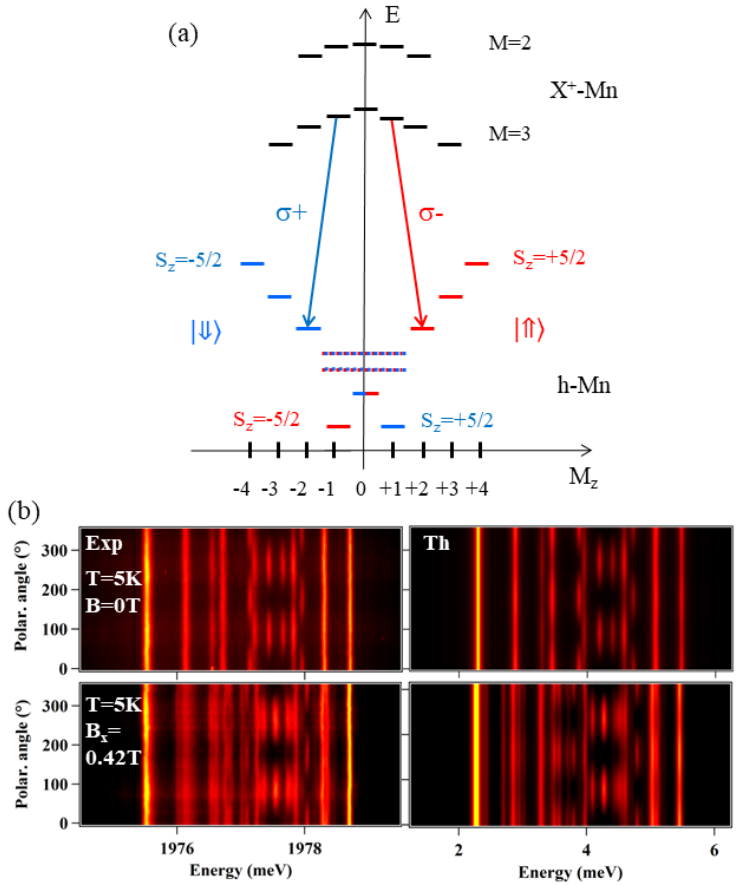

Figure I.3: (a) Energy levels of the ground (h-Mn) and excited (X^+-Mn) states in a positively charged Mn-doped quantum dot as a function of their angular momentum (M_z). The levels in dotted lines corresponds to the h-Mn states $|-1/2\rangle|\Uparrow_h\rangle$ and $|+1/2\rangle|\Downarrow_h\rangle$ coupled by the valence band mixing. Optical recombination towards these levels leads to linearly polarized lines. (b) Experimental (left) and calculated (right) color-scale plot of the linear polarization dependence of the PL of X^+-Mn of the QD presented in Fig. I.1 at B = 0 T (top) and $B_\perp$ = 0.42 T (bottom). The parameters used in the calculation are listed in Table I.1.

and, for the excited state (X^+-Mn):

$$\begin{aligned}\mathcal{H}_{X^+-Mn} &= \mathcal{H}^{ex}_{eMn} + 2\mathcal{H}_{scat} + \mathcal{H}_{CF,Mn} + \mathcal{H}_{mag,exc} \\ &= I_{eMn}\mathbf{S}.\boldsymbol{\sigma} - 2\eta S_z^2 + D_0 S_z^2 + E(S_x^2 - S_y^2) + g_{Mn}\mu_B \mathbf{S}.\mathbf{B} + g_e\mu_B\boldsymbol{\sigma}.\mathbf{B}\end{aligned} \tag{I.6}$$

The full energy structure given by those hamiltonian is presented in Fig. I.3, along with the linear polarization map of a QD. Values of I_{hMn}, I_{eMn}, ρ_c/Δ_{lh} and η for a

Table I.1: Values of the parameters used in the model of the positively charged Mn-doped QD presented in Fig. I.1. I_{eMn}, I_{hMn}, $\frac{\rho_s}{\Delta_{lh}}$, θ, η and T_{eff} are used to model the linear polarization intensity map of Fig. I.3. The other parameters cannot be extracted from the PL measurements and values for typical Mn-doped QDs are chosen for the calculation of the spin dynamics presented in Sec. I.2 and I.3.

I_{eMn}	I_{hMn}	$\frac{\rho_s}{\Delta_{lh}}$	θ	η	T_{eff}	g_e	g_h	g_{Mn}	D_0	E
μeV	μeV		$^\circ$	μeV	K				μeV	μeV
-175	345	0.09	0	30	20	-0.4	0.6	2	7	1.5

given QD can be obtained by comparing the linear polarization dependence of the experimental PL data to the optical transition probabilities calculated with the discussed effective spin model (Fig. I.3 (b)) [5]. A Boltzmann distribution function $P^i_{eMn} = e^{-E^i_{eMn}/k_B T_{eff}} / \sum_i e^{-E^i_{eMn}/k_B T_{eff}}$ with an effective spin temperature T_{eff} is used to describe the population of the emitting states (electron-Mn energy levels E^i_{eMn}). The extracted parameters are listed in Tab. I.1 for the QD presented in Fig. I.1 and I.3.

I.1.2 Resonant PL of X^+-Mn

Using a tunable continuous wave dye laser, a cross-polarized PLE map was acquired, detecting on the lower energy half of the spectra and scanning the higher energy lines in $\sigma+$ polarization. The results are presented in the inset of Fig. I.4 (a). We see three sharp emission lines, labelled (1), (2) and (3). These lines are strongly $\sigma-$ polarized, cross-polarized with the excitation, except (1) which is unpolarized. Those peaks appear when the laser is in resonance with specific QD transitions. We can associate a given high energy transition to each of the low energy peaks.

These linked transitions evidence Λ-level systems linking one excited state (e-Mn) to two ground states (h-Mn). All the e-Mn state can be written as $|M, M_z\rangle = \alpha|S_z, \uparrow_e\rangle + \beta|S_z - 1/2, \downarrow_e\rangle$. The first e-Mn state recombines toward the hole-Mn state $|S_z, \Downarrow_h\rangle$, emitting a photons in $\sigma-$ polarization, while the $|S_z - 1/2, \downarrow_e\rangle$ recombine with $|S_z - 1/2, \Uparrow_h\rangle$, emitting a photon in $\sigma+$ polarization. When an exciton is injected in the QD, the electron and Mn spins will be able to flip flop between those two states.

Using Fig. I.2, we can assign transitions observed in Fig. I.4 (a) to an electron-Mn state. They correspond, for a $\sigma+$ laser, to the successive resonant excitation of the electron-Mn levels $|3, +1\rangle$, $|3, +2\rangle$ and $|2, +2\rangle$, as shown in Fig. I.4 (b). These states are expressed as linear combinations of the Mn and electron spins $|S_z, \sigma_z\rangle$

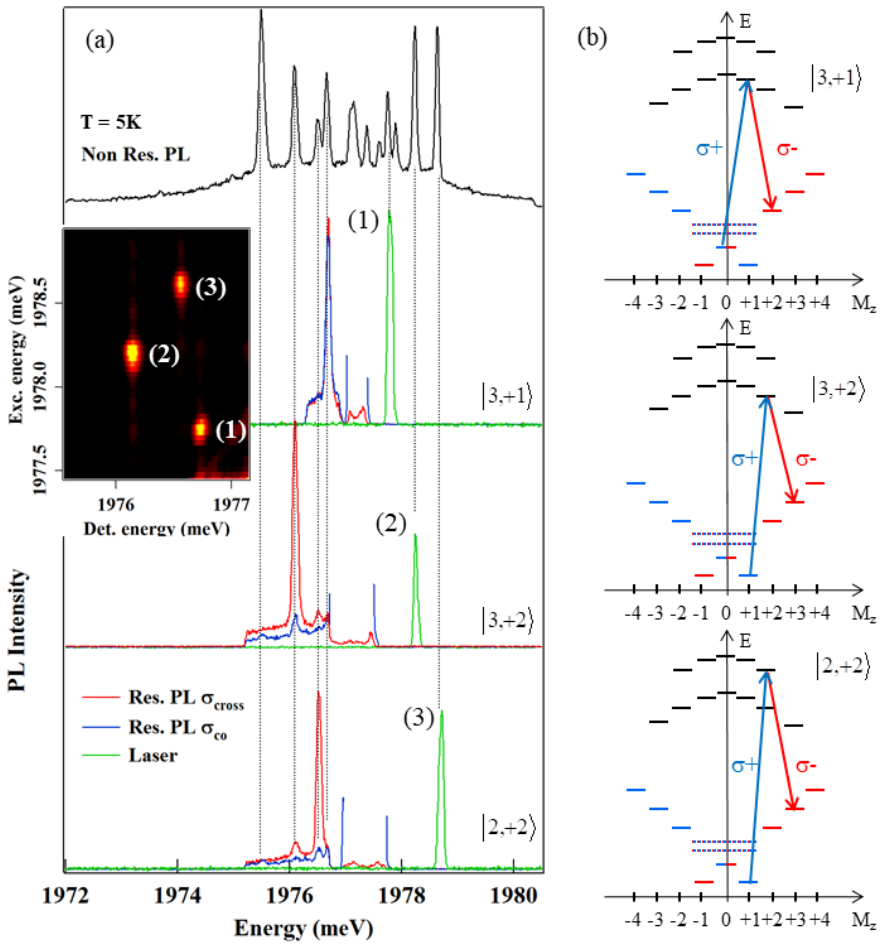

Figure I.4: (a) Non resonant (Non Res.) and resonant (Res.) PL of X^+-Mn. Co and cross circularly polarized PL spectra are collected for three different energies of the CW resonant laser (green). Inset: intensity map of the cross-circularly polarized PL detected on the low energy side of X^+-Mn as the CW laser is scanned through the high energy side. (b) Energy levels of X^+-Mn and identification of the three resonances observed in (a) corresponding to the optical Λ systems associated with the e-Mn states $|3,+1\rangle$, $|3,+2\rangle$ and $|2,+2\rangle$.

coupled by a flip-flop in Fig. I.2.

The energy splitting between the resonant absorption and the emission corresponds to the splitting between the two ground states of the Λ system. It is given by $4\times3/2I_{hMn}$($\approx$2.1 meV for the QD in Fig. I.2) for an excitation of $|3,+2\rangle$ or $|2,+2\rangle$ and $2\times3/2I_{hMn}$($\approx$1.05 meV for the QD in Fig. I.2) for an excitation of $|3,+1\rangle$. This is in good agreement with the previously determined value of I_{hMn}

For an excitation of $|3,+2\rangle$ or $|2,+2\rangle$, the weak co-polarized PL signal, which depends on the excitation intensity, comes from a possible direct excitation of the low energy branch of the Λ system through the acoustic phonon side-band [9].

I.2 Hole-Mn spin dynamics under resonant excitation

I.2.1 Cycling in and escaping from the Λ-level system

These Λ systems can be used to probe the dynamics of the hybrid h-Mn spin. Under resonant excitation of one of the branch, a fast optical pumping controlled by the generation rate and the radiative lifetime of the excited state is expected for an isolated Λ system: the population should be stored in the level which is not excited and the resonant PL should vanish. In the case of X^+-Mn, the PL intensity observed under resonant excitation of the high energy branch of the Λ systems is similar to the PL intensity obtained under non-resonant excitation. This suggests a very inefficient optical pumping of the hole-Mn spin and an efficient spin-flip mechanism which links the two ground states of the Λ systems.

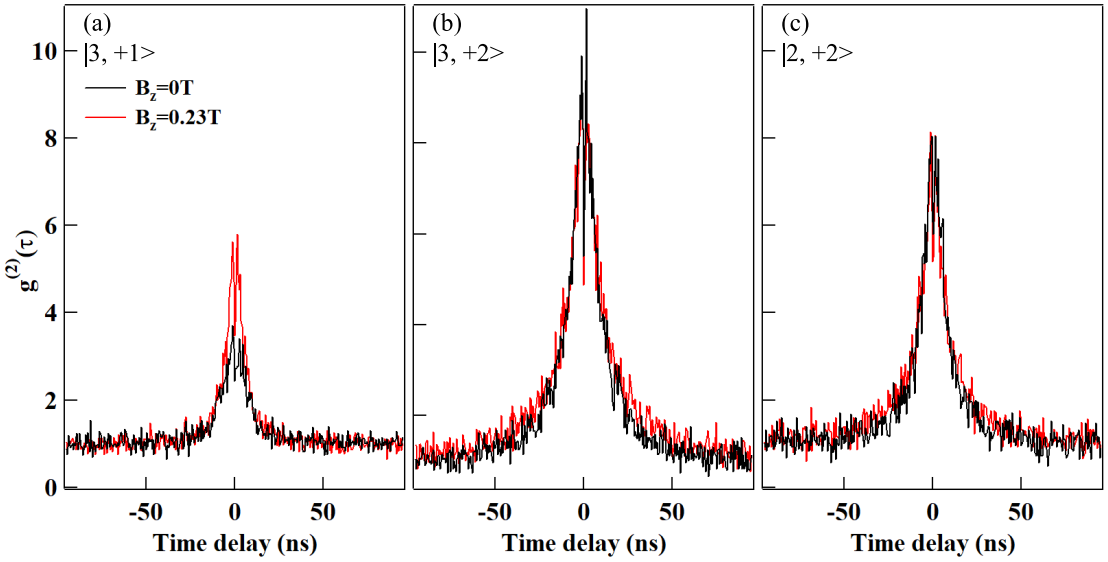

Figure I.5: Low temperature (T = 5 K) auto-correlation of the resonant PL for cross-circularly polarized excitation and detection of the electron-Mn states (a) $|3,+1\rangle$, (b) $|3,+2\rangle$ and (c) $|2,+2\rangle$.

The dynamics of the Mn spin coupled to carriers was first analyzed, under res-

onant optical excitation, through the statistics of the time arrival of the photons given by the second order correlation function of the resonant PL intensity. To access it, a Handury Brown and Twiss (HBT) setup was exploited with a resolution of about 0.8 ns to perform photon-correlation measurements. Under our experimental conditions, with photon count rates of a few kHz, the measured photon pair time distribution yields, after normalization, to the second order correlation function $g^{(2)}(\tau)$ of the PL intensity.

For the three resonant excitation conditions reported in Fig. I.5, $g^{(2)}(\tau)$ is mainly characterized by a large photon bunching with a full width at half maximum (FWHM) in the 20 ns range. The amplitude of the bunching reaches 9 for line (2) and is slightly weaker for the two other lines. This large bunching, reflecting an intermittency in the emission of the QD, is not sensitive to a longitudinal magnetic field B_z except for an excitation on (1).

The presence of a photon bunching is surprising at first: under resonant excitation of an isolated Λ system, an anti-bunching of the resonant PL controlled by the transfer time between the two ground states is indeed expected for a single emitter. For X^+-Mn, the observed short anti-bunching (dip near zero delay, better evidenced in Fig. I.5 (b)) suggests a fast transfer time in the nanosecond range between the two ground states of the Λ systems.

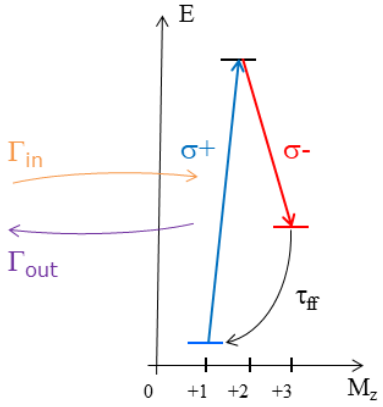

Figure I.6: Schema of the energy levels of the optical Λ system associated with the electron-Mn state $|3, +2\rangle$ extracted from the full level structure of a positively charged Mn-doped QD (Fig. I.4). The different processes discussed in this section are presented.

In the presence of a transfer process connecting the two hole-Mn ground states in a nanosecond time-scale (τ_{ff}), the photon bunching can be explained by leaks outside the resonantly excited Λ system. Under CW excitation, the population is cycled inside the Λ system until a spin flip occurs and drives the carrier-Mn spin out of the Λ levels under investigation. The resonant PL is then switched off until multiple spin-flips drives back the carriers and Mn spin inside the Λ system under excitation. The selected QD line can be either in a ON (populated) or OFF

(empty) state depending on the fluctuations of the carrier and Mn spins. The amplitude of the bunching is then given by Γ_{Out}/Γ_{In}, the ratio of the transition rates from OFF to ON (Γ_{In}) and from ON to OFF (Γ_{Out}). An amplitude of $g^{(2)}(\tau)$ than 1 is expected for the multilevel system considered here where, after a spin relaxation, multiple spin flips are in average required to come back to the initial state ($\Gamma_{In} < \Gamma_{Out}$). Thus the width of the bunching is a measurement of the escape time out of the Λ level system. We present these transitions in Fig. I.6, on the Λ system associated with $|3, +2\rangle$ state.

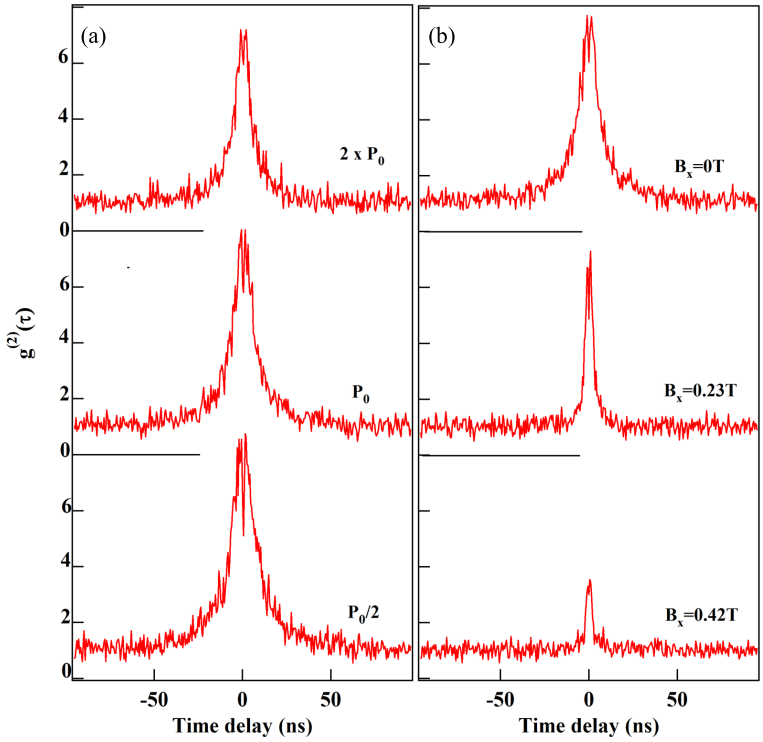

Figure I.7: Excitation power dependence (a) and transverse magnetic field dependence (b) at T = 5 K of the auto-correlation of the resonant PL obtained for an excitation on the high energy branch of the Λ level system associated to the e-Mn state $|2, +2\rangle$.

A weak transverse magnetic field, B_x, significantly reduces the width of the bunching signal (Fig.I.7 (b)). As the spin of the hole-Mn complex is highly anisotropic, with a large energy splitting induced by the exchange interaction $I_{hMn}S_z.J_z$, the weak transverse magnetic field mainly affects the electron-Mn dynamics in the excited state of the charged QD. Indeed, the transverse magnetic field couples the different electron-Mn states and induces a leak outside the resonantly excited Λ system. Both spin-flips within the hole-Mn (ground state) and

the electron-Mn (excited state) systems can contribute to the "bunching signal". The significant effect of the weak transverse field shows that the probability of presence in the excited state of the Λ system is large. This is consistent with the large excitation intensity used for these auto-correlation measurements which requires a high photon count rate.

A slight reduction of the width of the bunching signal is also observed with the increase of the excitation power (Fig.I.7 (a)). This shows that the leaks outside a given Λ system slightly increases with the probability of presence of the positively charged exciton in the QD.

I.2.2 Resonant optical pumping of the hole-Mn spin

Resonant optical pumping experiments were done to estimate how long it takes, after a spin-flip, for the hybrid hole-Mn spin to relax inside the resonantly excited Λ system. The experiments were performed using trains of circularly polarized light, prepared with an electro-optic or an acousto-optic modulator with a switching time of about 10 ns. The resonant PL was detected with a fast avalanche photodiode. Permanent magnet mounted on a translation stage were used to apply a weak magnetic field in Faraday (magnetic field parallel to the laser direction) or Voight (magnetic field perpendicular to the laser direction) configurations.

A demonstration of resonant optical pumping of the hole-Mn system was first done by exciting the high energy branch of the Λ systems with trains of resonant light, alternating the circular polarization and recording the circularly polarized PL of the low energy branch. As observed in Fig. I.8, for an excitation on resonance with the electron-Mn states $|3,+2\rangle$ or $|2,+2\rangle$, switching the polarization of the excitation from co to cross circular produces a change of the PL intensity with two transients: first, an abrupt PL increase, reflecting the population change of the observed spin-polarized charged excitons; then a slower transient with a characteristic time of a few tens of nanoseconds, depending on the laser excitation power.

The exponential decrease of the resonant PL intensity is the signature of an optical pumping of the hole-Mn spin: the hole-Mn state which is optically addressed is partially emptied when the population is transferred out of the excited Λ system. As presented in Fig. I.8, this pumping signal is not sensitive to a longitudinal magnetic field B_z except for an excitation of $|3,\pm1\rangle$ where B_z enhances the intensity difference between co and cross circular polarization.

The speed of the optical pumping increases with the excitation intensity. This is presented in Fig. I.9 (a) in the case of a resonant excitation of $|3,\pm2\rangle$ with alternate circular polarizations. At high excitation intensity, the pumping time saturates to a value similar to the width of the bunching signal observed in the auto-correlation measurements.

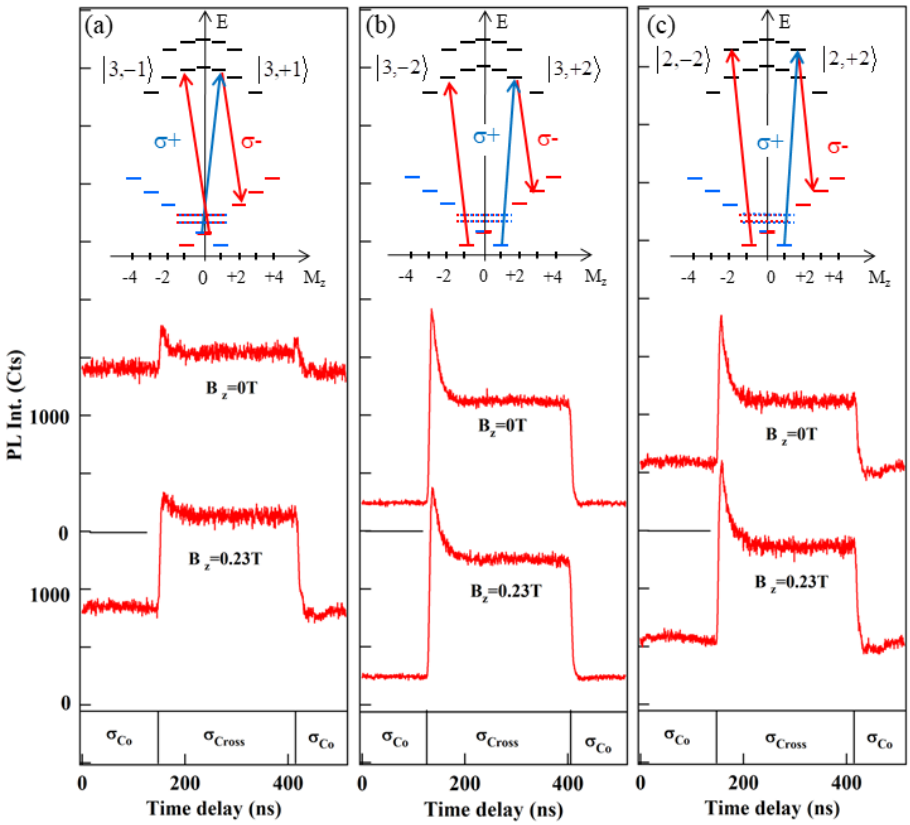

Figure I.8: Resonant optical pumping transients obtained at T = 5 K under circular polarization switching of the resonant excitation for the Λ systems associated with (a) $|3,+1\rangle$, (b) $|3,+2\rangle$ and (c) $|2,+2\rangle$ at zero field and under a weak longitudinal magnetic field B_z=0.23T. The insets present the corresponding states which are resonantly excited and detected in $\sigma-$ polarization.

As observed for the auto-correlation, the resonant pumping signal is also strongly sensitive to a transverse magnetic field. Under a weak transverse field (see Fig. I.9 (b)), we first observe an increase of the speed of the pumping together with a decrease of the amplitude of the signal when the transient time reaches the time resolution of the set-up (around 10 ns). For a large transverse field ($B_\perp$=0.42T), the co and cross circularly polarized resonant PL intensities are identical (see the inset of Fig. I.9 (b)) and similar pumping transients are observed when switching from σ_{co} to σ_{cross} or from σ_{cross} to σ_{co} circular polarization.

To measure the relaxation of the prepared non–equilibrium distribution of the hole-Mn spins, the circularly polarized pump laser is switched off during a dark time τ_{dark}. The amplitude of the pumping transient which appears after τ_{dark}

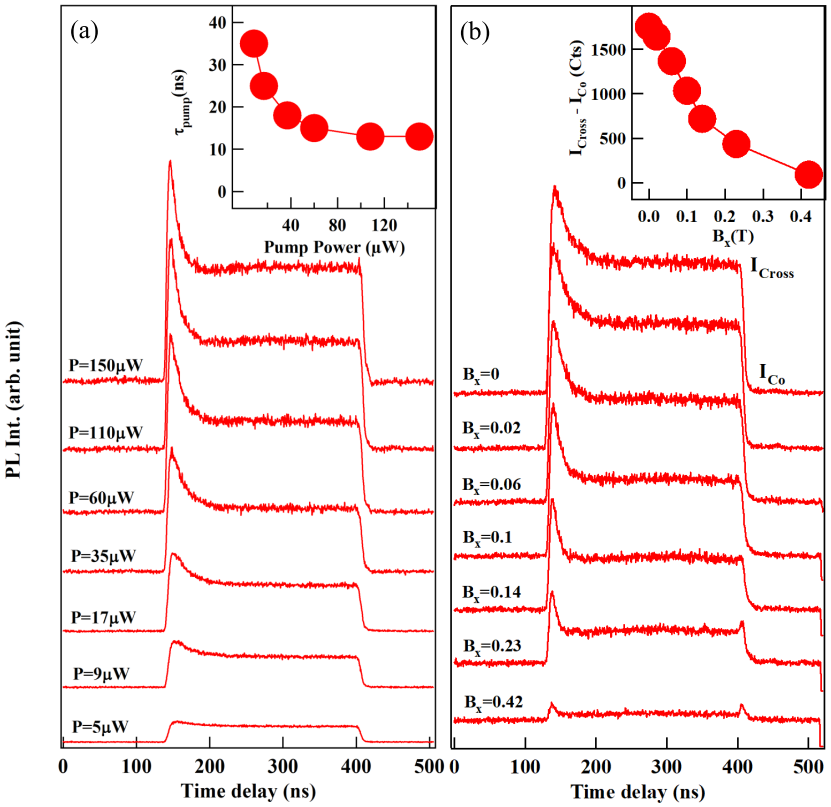

Figure I.9: Excitation power dependence (a) and transverse magnetic field dependence (b) of the optical pumping signal obtained for a resonant excitation on $|3, +2\rangle$ at T = 5 K. Insets: excitation power dependence of the pumping time (τ_{pump} and transverse magnetic field dependence of the difference of resonant PL intensity between σ_{cross} and σ_{co} excitation.

depends on the hole-Mn spin relaxation. A dark time of 50 ns is enough to observe the reappearance of a significant pumping transient (Fig. I.10). For comparison and for a better sensitivity of the measurement, the pumping transient observed in the absence of initial preparation of the hole-Mn spin (i.e. when switching of the circular polarization during the dark time) is also presented (red trace in Fig. I.10). The normalized difference of the amplitude of these two transients, $\Delta I/I$, as a function of τ_{dark} is presented in the inset of Fig.I.10. This measurement shows that, when the optical excitation is off, it takes around 80 ns for the hole-Mn spin to relax back to the ground state of the excited Λ system.

If the optical pumping would have stored the hole-Mn spin in the branch of the Λ system which is not optically excited, its characteristic time would be controlled by the exciton radiative lifetime and generation rate. With a hole-Mn relaxation

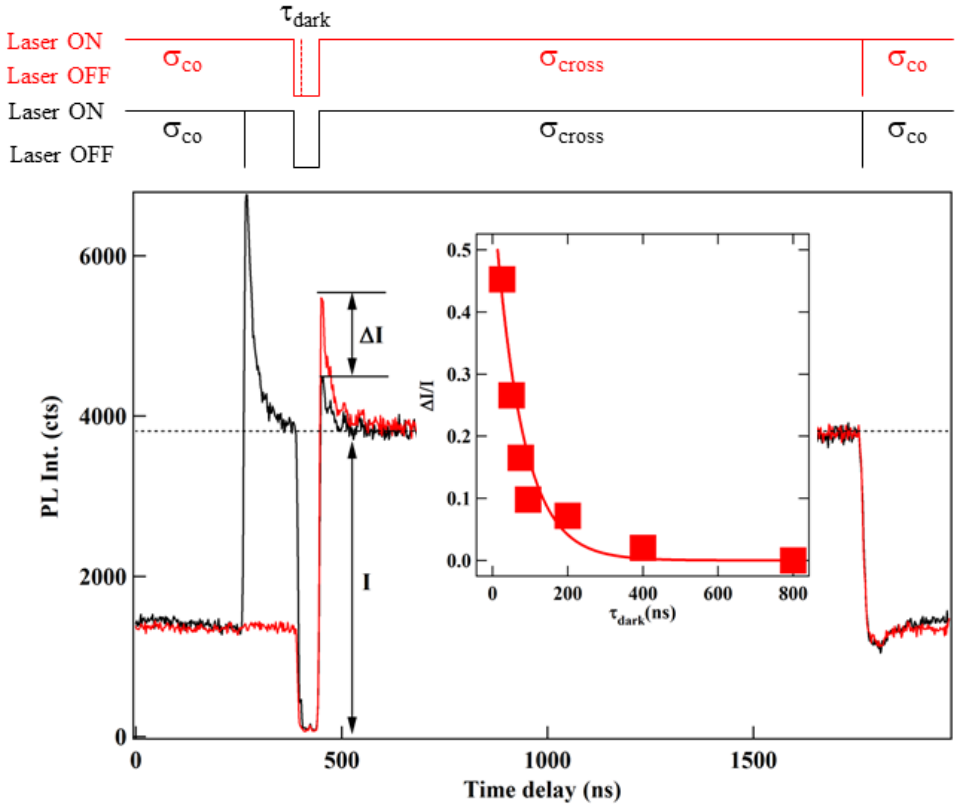

Figure I.10: Optical pumping experiment at T = 5 K for an excitation of $|3, +2\rangle$ with modulated circular polarization. A dark time ($\tau_{dark} = 50ns$) is introduced in the pumping sequence. The polarization switching occurs either before (black) or during (red) the dark time. The black and red diagrams present the corresponding resonant excitation sequences. Inset: variation of the ratio $\Delta I/I$ as a function of τ_{dark}. The solid line is an exponential fit with $\tau_{relax} = 80ns$.

time in the 100 ns range, as observed experimentally, the pumping should take place within a few nanoseconds.

Another source of spin pumping can be the leak outside the resonantly excited Λ system. In this case, the speed of the pumping is controlled by the leakage time and, as observed experimentally, the pumping time is similar to the width of the photon bunching signal. This mechanism of pumping for the hole-Mn spin is confirmed by the transverse magnetic field dependence. The acceleration of the optical pumping in transverse magnetic field (Fig. I.9 (b)) has the same origin as the decrease of the width of the bunching signal. By mixing the different electron-Mn states, the transverse field enhances the leakage probability out of the resonantly driven Λ system and decreases the corresponding optical pumping

time.

I.2.3 Modelling of spin relaxation mechanism: hole-Mn flip-flops mediated by a lattice deformation

The observed large resonant PL amplitude of X^+-Mn and its dynamics can be qualitatively explained if a fast (nanosecond) and efficient spin transfer mechanism connects the two hole-Mn ground states of each Λ system. This transfer time is noted τ_{ff}. We propose a mechanism for the hole-Mn flip-flop at low temperature resulting from a deformation induced exchange interaction [10, 11]. We show here that hole-Mn states are efficiently coupled via the interplay of their exchange interaction and the lattice deformation induced heavy-hole/light-hole mixing. We will focus in the following on the two hole-Mn states $|+\frac{3}{2};\Uparrow_h\rangle$ and $|+\frac{5}{2};\Downarrow_h\rangle$ in the ground states of the Λ system associated with the electron-Mn levels $|3,+2\rangle$ and $|2,+2\rangle$. Similar results could be obtained with the hole-Mn ground states of the other Λ systems.

First, let us notice that the non diagonal term of the hole-Mn exchange interaction $\frac{I_{hMn}}{2}(S^+J^- + S^-J^+)$ couples the heavy-holes $(\Uparrow_h, \Downarrow_h)$ and light-holes $(\uparrow_h, \downarrow_h)$ levels split by Δ_{lh} through a hole-Mn flip-flop. We consider this interaction as a perturbation on the Mn heavy-hole level structure given by $I_{hMn}S_zJ_z$. As presented in Sec. I.1.5, we can rewrite the two perturbed ground states $|+\widetilde{\frac{3}{2};\Uparrow_h}\rangle$ and $|+\widetilde{\frac{5}{2};\Downarrow_h}\rangle$ of the Λ system as:

$$\begin{aligned} |+\widetilde{\frac{5}{2};\Downarrow_h}\rangle &= |+\frac{5}{2};\Downarrow_h\rangle - \frac{\sqrt{15}}{2}\frac{I_{hMn}}{\Delta_{lh}}|+\frac{3}{2};\downarrow_h\rangle \\ |+\widetilde{\frac{3}{2};\Uparrow_h}\rangle &= |+\frac{3}{2};\Uparrow_h\rangle - \frac{\sqrt{15}}{2}\frac{I_{hMn}}{\Delta_{lh}}|+\frac{5}{2};\uparrow_h\rangle \end{aligned} \tag{I.7}$$

where we neglect the exchange energy shifts of the hole-Mn levels much smaller than Δ_{lh}.

Phonon-induced deformations comes into play via the off-diagonal terms of the Bir-Pikus Hamiltonian $\mathcal{H}_{BP}$, describing the influence of strain on the valence band, as written in Eq. **??**. The strain produced by phonon vibrations couples the perturbed hole-Mn states $|+\widetilde{5/2}\Downarrow_h\rangle$ and $|+\widetilde{3/2}\Uparrow_h\rangle$ through the Hamiltonian term

$$\langle+\widetilde{\frac{5}{2};\Downarrow_h}\,|H_{BP}|+\widetilde{\frac{3}{2};\Uparrow_h}\rangle = 2\times(-\frac{\sqrt{15}}{2}\frac{I_{hMn}}{\Delta_{lh}})\times R^* \tag{I.8}$$

Table I.2: Material (CdTe or ZnTe) [12] and QD parameters used in the calculation of the coupled hole and Mn spin relaxation time.

CdTe		
Deformation potential constants	$\|b\|$	-1.0 eV
	$\|d\|$	-4.4 eV
Longitudinal sound speed	c_l	3300 m/s
Transverse sound speed	c_t	1800 m/s
Density	ρ	5860 kg/m^3
ZnTe		
Deformation potential constants	$\|b\|$	-1.4 eV
	$\|d\|$	-4.4 eV
Longitudinal sound speed	c_l	3800 m/s
Transverse sound speed	c_t	2300 m/s
Density	ρ	5908 kg/m^3
Quantum dot		
Hole Mn exchange energy	I_{hMn}	0.35 meV
hh-lh exciton splitting	Δ_{lh}	15 meV
Hole wave function widths:		
- in plane	$l_\perp$	3.0 nm
- z direction	l_z	1.25 nm

with R a deformation dependent non-diagonal term of $\mathcal{H}_{BP}$ [10, 11] written

$$R = \frac{\sqrt{3}}{2} b(\epsilon_{xx} - \epsilon_{yy}) - id\epsilon_{xy} \tag{I.9}$$

with b and d given in Tab. I.2 for CdTe and ZnTe. The coupling of the hole-Mn states results from an interplay between the hole-Mn exchange interaction and the deformation: neither the exchange interaction nor the deformation perturbation alone can couple these states.

According to Eq. I.8, the effective Hamiltonian describing the interaction mechanism with phonons in the subspace $\{|+\frac{5}{2};\Uparrow_h\rangle, |+\frac{5}{2};\Downarrow_h\rangle, |+\frac{3}{2};\Uparrow_h\rangle, |+\frac{3}{2};\Downarrow_h\rangle\}$ is

$$H_{int} = -\sqrt{15}\frac{I_{hMn}}{\Delta_{lh}} R^* |+\frac{5}{2};\Downarrow_h\rangle\langle+\frac{3}{2};\Uparrow_h| + H.c \tag{I.10}$$

The spin decay rates from $|+\frac{3}{2};\Uparrow_h\rangle$ to $|+\frac{5}{2};\Downarrow_h\rangle$ accompanied by the emission of an acoustic phonon is given by Fermi's golden rule

$$\tau^{-1} = \frac{2\pi}{\hbar} \sum_k \left| \langle +\frac{5}{2};\Downarrow_h;\psi;n_k+1|H_{int}|+\frac{3}{2};\Uparrow_h;\psi;n_k\rangle \right|^2 \times \delta(\hbar\omega_0 - \hbar\omega_k) \tag{I.11}$$

where $\hbar\omega_0$ is the energy splitting between $|+\frac{5}{2};\Downarrow_h\rangle$ and $|+\frac{3}{2};\Uparrow_h\rangle$, n_k the number of phonons in mode k and ψ the orbital part of the hole wave function.

To evaluate the matrix element in Eq. I.11 we use the strain tensor components ϵ_{ij} given by

$$\epsilon_{ij} = \frac{1}{2}\left(\frac{\partial u_i}{\partial r_j} + \frac{\partial u_j}{\partial r_i}\right) \tag{I.12}$$

where $\mathbf{u}(\mathbf{r})$ is the local displacement field. For an acoustic phonon, the quantized displacement field can be written in the real space [11, 13]:

$$\mathbf{u}(\mathbf{r}) = i\sum_{k,\lambda}\sqrt{\frac{\hbar}{2\rho\omega_{k,\lambda}N\nu_0}}\mathbf{e}_{k,\lambda}(b_{k,\lambda} + b^{\dagger}_{-k,\lambda})\exp(i\mathbf{kr}) \tag{I.13}$$

where N is the number of unit cells in the crystal, ν_0 is the volume of a cell and ρ the mass density. $b^{\dagger}_{k,\lambda}$ ($b_{k,\lambda}$) is the creation (annihilation) operator of phonon in the mode (k,λ) of energy $\hbar\omega_{k,\lambda}$ and $\mathbf{e}_{k,\lambda}$ is the unit polarization vector. In zinc-blend crystals there are two transverse acoustic phonon branches $\lambda = t_1, t_2$ and one longitudinal acoustic phonon branch $\lambda = l$. The polarization vectors of these phonons branches are given by [14]:

$$\begin{aligned}
\mathbf{e}_{k,l} &= \frac{\mathbf{k}}{k} = \frac{1}{k}(k_x, k_y, k_z) \\
\mathbf{e}_{k,t_1} &= \frac{1}{kk_\perp}(k_x k_z, k_y k_z, -k_\perp^2) \\
\mathbf{e}_{k,t_2} &= \frac{1}{k_\perp}(k_y, -k_x, 0)
\end{aligned} \tag{I.14}$$

with $k_\perp = \sqrt{k_x^2 + k_y^2}$.

Using Eq. I.12, I.13 and I.14, we calculate the matrix element in Eq.I.11:

$$\begin{aligned}
|M_{k,\lambda}|^2 = \; & 15\left(\frac{I_{hMn}}{\Delta_{lh}}\right)^2 \frac{\hbar}{2\rho\omega_{k,\lambda}N\nu_0}\left(n_B(\omega_{k,\lambda}) + 1\right) \\
& \times\left(\frac{3b^2}{4}(k_x e_{x,\lambda} - k_y e_{y,\lambda})^2 + \frac{d^2}{4}(k_x e_{y,\lambda} + k_y e_{x,\lambda})^2\right) \times |\mathcal{F}_\lambda(\mathbf{k})|^2
\end{aligned} \tag{I.15}$$

with

$$\mathcal{F}_\lambda(\mathbf{k}) = \int_{-\infty}^{\infty} d^3r\psi^*(\mathbf{r})\exp(i\mathbf{kr}\psi(\mathbf{r})) \tag{I.16}$$

and $n_B(\omega_{k,\lambda}) = 1/(e^{\hbar\omega_{k,\lambda}/K_BT} - 1)$, the thermal phonon distribution function.

For a Gaussian hole wave function with in-plane and z-direction parameters $l_\perp$ and l_z respectively (full width at half maximum $2\sqrt{2\ln 2}l_i$) we have

$$\psi(\mathbf{r}) = \frac{1}{\pi^{3/4} l_\perp \sqrt{l_z}} \exp\left(-\frac{1}{2}\left(\left(\frac{r_\perp}{l_\perp}\right)^2 + \left(\frac{z}{l_z}\right)^2\right)\right) \tag{I.17}$$

Then, the form factor $\mathcal{F}_\lambda(\mathbf{k})$, which is the Fourier transform of $|\psi(\mathbf{r})|^2$, becomes

$$\mathcal{F}_\lambda(\mathbf{k}) = \exp\left(-\frac{1}{4}\left((l_\perp k_\perp)^2 + (l_z k_z)^2\right)\right) \tag{I.18}$$

Considering a linear dispersion of acoustic phonons $\omega_{k,\lambda} = c_\lambda k$ and in spherical coordinates with $\mathbf{k} = k(\sin\theta\cos\varphi, \sin\theta\sin\varphi, \cos\theta)$ Eq. I.11 reads:

$$\begin{aligned} \tau^{-1} = \; & \sum_\lambda \frac{15}{(2\pi)^2}\left(\frac{I_{hMn}}{\Delta_{lh}}\right)^2 \left(\frac{\omega_0}{c_\lambda}\right)^3 \frac{1}{2\hbar\rho c_\lambda^2}\frac{\pi}{4}(3b^2+d^2) \\ & \times (n_B(\omega_0)+1)) \int_0^\pi d\theta \sin\theta |\mathcal{F}_\lambda(\omega_0,\theta)|^2 G_\lambda(\theta) \end{aligned} \tag{I.19}$$

where we used the continuum limit ($\sum_k \to V/(2\pi)^3 \int d^3k$ with $V = N\nu_0$ the crystal volume) and integrated over k and φ. The summation is taken over the acoustic phonon branches λ of corresponding sound velocity c_λ. The geometrical form factors of each phonon branch $G_\lambda(\theta)$ is given by

$$\begin{aligned} G_l(\theta) &= \sin^4\theta \\ G_{t_1}(\theta) &= \sin^2\theta\cos^2\theta \\ G_{t_2}(\theta) &= \sin^2\theta \end{aligned} \tag{I.20}$$

In the numerical calculation of the spin flip time τ_{ff} presented in Fig.I.11 we used the material parameters of CdTe, ZnTe and the self-assembled CdTe/ZnTe QDs listed in Table I.2. The calculated relaxation time strongly depends on the energy separation between the hole-Mn levels $\hbar\omega_0$. This energy dependence is controlled by the size of the hole wave-function given by $l_\perp$ and l_z. The estimated flip-flop time is also strongly sensitive to the exchange induced mixing of the ground heavy-hole states with the higher energy light-hole levels. In the model presented here, this mixing is controlled by Δ_{lh}, the effective energy splitting between heavy-holes and light-holes. This parameter can describe more complex effects such as a coupling of the confined heavy-hole with ground state light-holes in the barriers [15] or an effective reduction of heavy-hole/light-hole splitting due to a presence of a dense manifold of heavy-hole like QD states lying between the confined heavy-hole and light-hole levels [16]. From this modelling it is deduced that, for a hole confined in small $Cd_xZn_{1-x}Te$ alloy QDs, the hole-Mn flip-flop time τ_{ff} can easily be bellow 2 ns for an effective heavy-hole/light-hole splitting $\Delta_{lh} = 15$ meV and an energy splitting $\hbar\omega_0$ in the meV range. The value of $\tau_{ff} = 1.5$ ns will be used for the ground states of each Λ system.

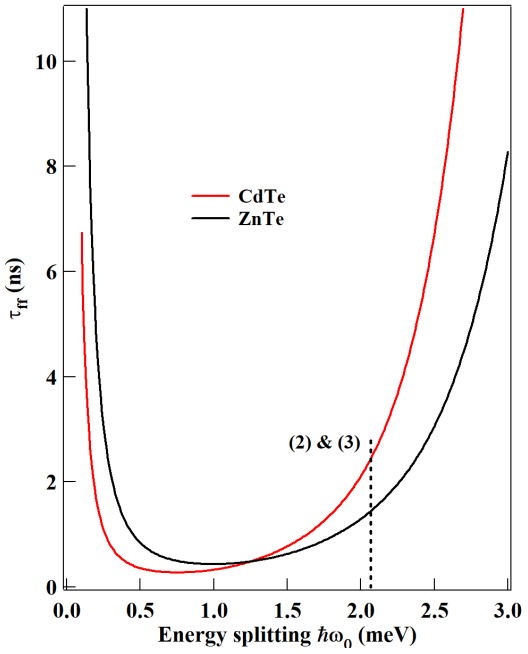

Figure I.11: Relaxation time τ_{ff}, between the two hole-Mn ground states of the Λ system calculated with the parameters listed in Table I.2 at a temperature T = 7 K. The doted line shows the energy splitting of the hole-Mn states involved in the Λ systems considered here (Resonances (2) and (3) identified in Fig. I.4).

I.2.4 Model of the carrier-Mn spin dynamics under resonant excitation

Using the level scheme presented in Fig. I.3 (a) for a positively charged Mn-doped QD and the estimated hole-Mn flip-flop rates, we calculated the time evolution of the 24 × 24 density matrix ϱ describing the population and the coherence of the 12 electron-Mn states in the excited state and the 12 hole-Mn states in the ground state of a positively charged QD. In the Markovian approximation, the master equation which governs the evolution of ϱ can be written in a general form (Lindblad form) as:

$$\frac{\partial \varrho}{\partial t} = \frac{-i}{\hbar}[\mathcal{H}, \varrho] + L\varrho \tag{I.21}$$

where $\mathcal{H}$ is the Hamiltonian of the complete system hole-Mn, $\mathcal{H}_{hMn}$, and X^+-Mn, $\mathcal{H}_{X^+Mn}$, as described in Eq. I.5 and I.6.

In Eq. I.21, $L\varrho$ describes the coupling or decay channels resulting from an interaction with the environment [17–19]. The population transfers from level j to level i in an irreversible process associated with a coupling to a reservoir is described by a Lindblad term of the form

$$L_{inc,j\to i}\varrho = \frac{\Gamma_{j\to i}}{2}(2|i\rangle\langle j|\varrho|j\rangle\langle i| - \varrho|j\rangle\langle j| - |j\rangle\langle j|\varrho) \tag{I.22}$$

where $\Gamma_{j\to i}$ is the incoherent relaxation rate from level j to level i. Such term can describe the radiative decay of the exciton (irreversible coupling to the photon modes) or the relaxation of the carriers or Mn spin (irreversible coupling to the phonon modes). It can also be used to describe the optical generation of an exciton in the low excitation regime where the energy shift induced by the coupling with the laser field is neglected.

A pure dephasing (i.e. without exchange of energy with a reservoir) can also be introduced for the different spins and described by $L_{deph,jj}\varrho$:

$$L_{deph,jj}\varrho = \frac{\gamma_{jj}}{2}(2|j\rangle\langle j|\varrho|j\rangle\langle j| - \varrho|j\rangle\langle j| - |j\rangle\langle j|\varrho) \tag{I.23}$$

where γ_{jj} is the pure dephasing rate of level j.

To identify the main spin relaxation channels responsible for the observed spin fluctuations, we first modelled the auto-correlation of the resonant PL using the full spin level structure of a p-doped magnetic QD. For a qualitative description of the observed spin dynamics, we used as an example the Mn-doped QD parameters listed in Tab. I.1 and reasonable order of magnitude for the spin relaxation times, listed in Fig. I.12.

We considered that the spin dynamics in the excited state is controlled by the time evolution of $\mathcal{H}_{X^+Mn}$, the generation rate of excitons $\gamma_g = 1/\tau_g$ and their radiative lifetime $\tau_r = 0.3$ ns. The coherence of the coupled electron-Mn spins is limited by a pure dephasing term $T_2^{eMn} = 0.5$ ns, extracted from the time resolved PL (see Sec. I.3).

For the hole-Mn system in the ground state, we take into account a spin relaxation time of the Mn in the exchange field of the hole, τ_{Mn}, describing the relaxation channels involving a change of the Mn spin by one unit. This spin relaxation channel was introduced for a general description, however its characteristic time (in the μs range) is long compared to the time-scale of the dynamics considered in the resonant PL experiments and does not qualitatively affect the calculated time evolution.

Because of the presence of VBM, the spin flip of the hole independently of the Mn is expected to be more efficient. A spin flip time in the 10 ns range has been calculated for a hole in the exchange field of a Mn [20, 21]. A relaxation time of the hole spin around 5 ns has also been measured in negatively charged CdTe/ZnTe QDs in the absence of magnetic field [22]. Possible spin flips of the hole by one unit with a characteristic time $\tau_h = 10$ ns were also included in the model. The phonon induced hole-Mn flip-flops, occurring at τ_{ff}, are also introduced between the two hole-Mn ground states of each Λ system.

For a general qualitative description, an additional pure dephasing time T_2^{hMn} was also included in the dynamics of the hole-Mn system with a Lindblad term in the form of Eq. I.23. We cannot extract this parameter from the experiments. We

chose $T_2^{hMn} = 5ns$, slightly longer than what was measured for electron-Mn, as the hole-Mn system is highly split and less sensitive to effective fluctuating magnetic field such as the one produced by nuclear spins [22, 23].

The transition rates $\Gamma_{\gamma\to\gamma'}$ between the different hole-Mn states depend on their energy separation $E_{\gamma\gamma'} = E_{\gamma'} - E_{\gamma}$. Here we used $\Gamma_{\gamma\to\gamma'} = 1/\tau_i$ if $E_{\gamma\gamma'} < 0$ and $\Gamma_{\gamma\to\gamma'} = 1/\tau_i e^{-E_{\gamma\gamma'}/k_BT}$ if $E_{\gamma\gamma'} > 0$ [20, 24]. This accounts for a thermalization among the 12 hole-Mn levels with an effective spin temperature T. The optical excitation (τ_g), the exciton recombination (τ_r), the Mn spin relaxation (τ_{Mn}), the hole spin relaxation (τ_h) and the phonon induced transfer time (τ_{ff}) produce an irreversible population transfer between the γ and γ' levels and are described by Lindblad terms (Eq. I.22).

To model the auto-correlation of the $\sigma-$ PL intensity of the electron-Mn state $|3;+2\rangle$ under CW $\sigma+$ resonant excitation, we used the density matrix formalism and calculated the time evolution of $\rho_{|+\frac{3}{2};\uparrow_e\rangle}(t)$ with the initial condition $\rho_{|+\frac{3}{2};\Uparrow_h\rangle}(0) = 1$. The initial condition corresponds to the hole-Mn spin being in the state $|+\frac{3}{2};\Uparrow_h\rangle$ just after the emission of a $\sigma-$ photon on the low energy branch of the Λ system. This is a slight approximation: in the presence of VBM, the two ground states of a given Λ system are not completely pure hole-Mn spin states but are slightly coupled by a hole-Mn flip-flop induced by the exchange interaction $\mathcal{H}_{hMn}^{ex}$. However, since the splitting between the $|+\frac{3}{2};\Uparrow_h\rangle$ and $|+\frac{5}{2};\Downarrow_h\rangle$ states ($\Delta = 4\times 3/2 I_{hMn}$) is large compared to the coupling term ($W = \sqrt{15}\frac{\rho_c}{\Delta_{lh}} I_{hMn}$), their coherent coupling is weak. With a large valence band mixing $\frac{\rho_c}{\Delta_{lh}} = 0.1$, as observed in the dot discussed in this paper, the population of the hole-Mn system initialized in the state $|+\frac{3}{2};\Uparrow_h\rangle$ oscillates rapidly between the two corresponding hole-Mn ground states of the Λ system with a maximum amplitude of about 1.6% and an average population transfer efficiency of 0.8% [25]. Under resonant excitation on the high energy branch of the the Λ system, the QD remains OFF more than 99% of the time. As we will see in the following, the contribution of this weak coherent population transfer to the auto-correlation signal is not significant.

$\rho_{|+\frac{3}{2};\uparrow_e\rangle}(t)$ obtained with the QD parameters listed in Tab. I.1 is presented in Fig. I.12 (a). This quantity has to be normalized by $\rho_{|+\frac{3}{2};\uparrow_e\rangle}(\infty)$) to show the calculated autocorrelation signal. After a fast increase, the calculated population presents a maximum at short delay (t $<$ 5 ns). This model is based on a large number of parameters, whose values cannot all be extracted precisely from the measurements. However, with the spin relaxation parameters given in the caption of Fig. I.12, the width and the amplitude of the maximum are in good agreement with the photon bunching signals observed experimentally.

The width of the calculated bunching is controlled by all the spin-flip terms that can induce an escape out of the resonantly excited Λ system. At zero transverse magnetic field, it is dominated by spin flips in the hole-Mn system. If we put the

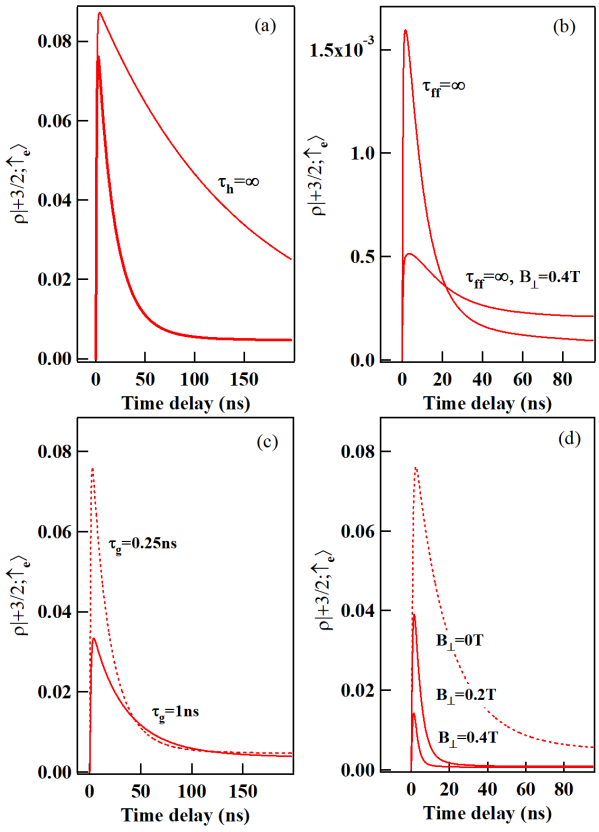

Figure I.12: Calculated time evolution of $\rho_{|+\frac{3}{2},\uparrow_e\rangle}(t)$ with the QD parameters listed in Table I.1 and, unless specified on the figure, τ_r=0.3ns, τ_{Mn}=5 μs, τ_h=10ns, τ_g=0.25 ns, τ_{ff}=1.5 ns, T_2^{hMn}= 5 ns, T_2^{eMn}= 0.5 ns, T=10K and B$_\perp$=0. (a) shows the results of the calculation with the above parameters and the influence of τ_h. (b), (c) and (d) illustrate the influence of, respectively, τ_{ff}, τ_g and $B_\perp$ on $\rho_{|+\frac{3}{2},\uparrow_e\rangle}(t)$. Note the different vertical scale in (b).

hole spin relaxation time as infinite ($\tau_h \to \infty$), $\rho_{|+\frac{3}{2};\uparrow_e\rangle}(t)$ is only controlled by the evolution of the hamiltonian $\mathcal{H}_{X^+-Mn}$ and the decoherence. The time evolution of $|+\frac{3}{2};\uparrow_e\rangle$, illustrated in Fig. I.12 (a), becomes then much slower than observed experimentally (Fig. I.7).

The dependence of $\rho_{|+\frac{3}{2};\uparrow_e\rangle}(t)$ on the excitation intensity, τ_g, and transverse magnetic field, $B_\perp$, are also well reproduced by the model (Fig. I.12 (c) and (d) respectively). At zero magnetic field, the leaks outside the excited Λ systems are dominated by τ_h. $\mathcal{H}_{X^+-Mn}$ induces fluctuations in a slightly longer time scale, as can be seen on Fig. I.12(a) for $\tau_h \to \infty$. The situation is different under a weak transverse magnetic field where the electron-Mn states are mixed, introducing new

channel of escape and significantly reducing the width of the photon bunching (See Fig. I.7 for the corresponding experiments).

Suppressing the fast flip-flop process connecting the two hole-Mn ground states ($\tau_{ff} = \infty$ in Fig. I.12 (b)) still produces a bunching as with the initial condition used in the calculation ($\rho_{|+\frac{3}{2};\Uparrow_h\rangle}(0) = 1$): a weak coherent transfer between the two ground states of the Λ system still exists. However, with this weak transfer only, the calculated PL intensity is always more than 50 times smaller than with τ_{ff}. The contribution of this weak process to the calculated auto-correlation signal (Fig. I.12 (a)) can therefore be safely neglected, and we can consider the phonon mediated relaxation to be the main transfer process in the Λ system.

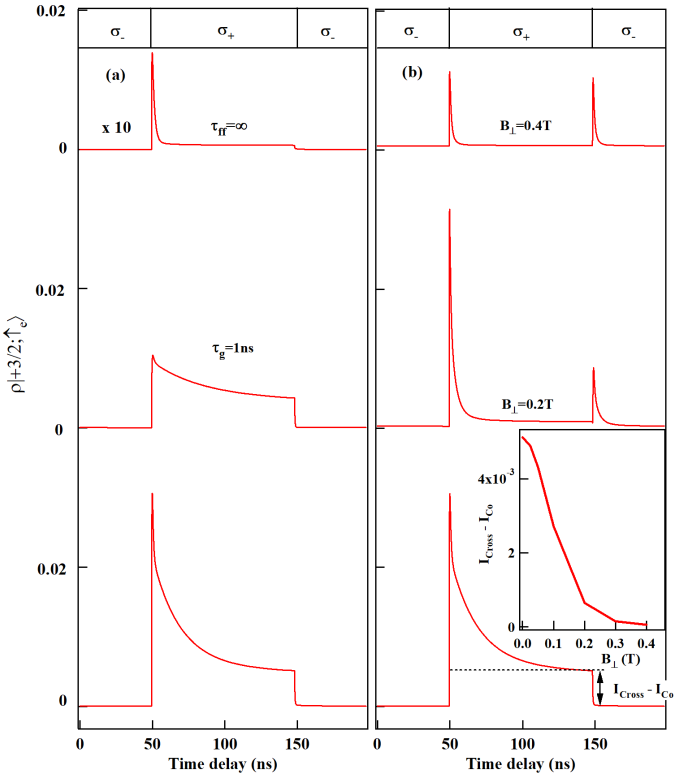

Figure I.13: Calculated resonant optical pumping transients for a $\sigma-$ detection and an excitation of $|3,+2\rangle$ and $|3,-2\rangle$ with modulated circular polarization. The QD parameters for the calculations are those listed in Tab. I.1 and τ_r=0.3 ns, τ_{Mn}=5 μs, τ_h=10 ns, T_2^{hMn}= 5 ns, T_2^{eMn}= 0.5 ns, τ_{ff}=1.5 ns, T=10 K and τ_g=0.25 ns. (a) Influence of a variation of τ_g and τ_{ff}. (b) Influence of a transverse magnetic field $B_\perp$. The inset presents the transverse magnetic field dependence of the difference of population for a $\sigma+$ or a $\sigma-$ excitation.

With this model, we can also calculate the population of the electron-Mn states

under resonant excitation with alternated circular polarization and estimate the efficiency and dynamics of the optical pumping. Fig. I.13 presents the time evolution of the population of the electron-Mn state $|+\frac{3}{2},\uparrow_e\rangle$ under alternated resonant excitation of $|3,+2\rangle$ in $\sigma+$ polarization or $|3,-2\rangle$ in $\sigma-$ polarization. This corresponds to the experimental configuration where the QD is resonantly excited with modulated circular polarization at the energy of $|3,+2\rangle$ and $|3,-2\rangle$ (absorption (2) in Fig. I.4 (b)) and the low energy resonant PL is detected in $\sigma-$ polarisation. The main features of the time-resolved optical pumping experiments (see Fig. I.8 and Fig. I.9) are well reproduced by the model. The timescale of the pumping transient, in the few tens of nanosecond range, and its excitation intensity dependence are also in good agrement with the experiments (see Fig. I.13 (a)).

The influence of a transverse magnetic field, $B_\perp$, on the optical pumping transient is also well described by this model. First, a significant reduction of the pumping time is observed for a weak magnetic field ($B_\perp = 0.2$ T in Fig. I.13(b)). As for the autocorrelation, this acceleration comes from the increase of the leakage out of the Λ system induced by the mixing of the electron-Mn states. Secondly, the transients obtained when switching the polarization from σ_{co} to σ_{cross} and from σ_{cross} to σ_{co} become identical for $B_\perp \approx 0.4$T, as observed in the experiments (Fig. I.9 (b)).

To understand this behaviour under $B_\perp$, let us remember that we resonantly excite $|3,+2\rangle$ from $|+\frac{5}{2},\Downarrow_h\rangle$ with $\sigma+$ light and excite $|3,-2\rangle$ from $|-\frac{5}{2},\Uparrow_h\rangle$ with $\sigma-$ photons. In both cases we detect the population of $|+\frac{3}{2},\uparrow_e\rangle$ in $\sigma-$ polarization (see the excitation/detection configuration illustrated in the inset of Fig. I.8 (b)). If the states $|3,+2\rangle$ and $|3,-2\rangle$ are uncoupled, as it is the case at zero field, we do not detect any light during the $\sigma-$ excitation. With a sufficiently large mixing of $|3,+2\rangle$ and $|3,-2\rangle$ induced by the transverse magnetic field, for a $\sigma-$ excitation of $|3,-2\rangle$, the population can be coherently transferred to $|3,+2\rangle$ during the charged exciton lifetime and $\sigma-$ light is detected after a recombination towards $|+\frac{3}{2},\Uparrow_h\rangle$ (see Sec. I.3). In the optical pumping sequence, we can then observe, in $\sigma-$ polarization, a transient when the $\sigma+$ excitation empties the state $|+\frac{5}{2},\Downarrow_h\rangle$ but also a similar transient when the $\sigma-$ excitation empties the state $|-\frac{5}{2},\Uparrow_h\rangle$. The transverse magnetic field dependence of the difference of steady state intensity observed in σ_{co} and σ_{cross} polarization (inset of Fig. I.9 (b)) is also well reproduced by the model (inset of Fig. I.13 (b)). This depolarization curve is controlled by the anisotropy of the electron-Mn spin that is induced by η and D_0 [5]. Finally, as expected, suppressing τ_{ff} from the model, a very weak average resonant PL and a fast optical pumping are obtained (Fig. I.13 (a), top curve).

Including a dark time in the pumping sequence, we can numerically evaluate the time required for the hole-Mn spin to return to the ground state of the excited Λ system. The time evolution of the population of the hole-Mn state $|+5/2,\Downarrow_h\rangle$

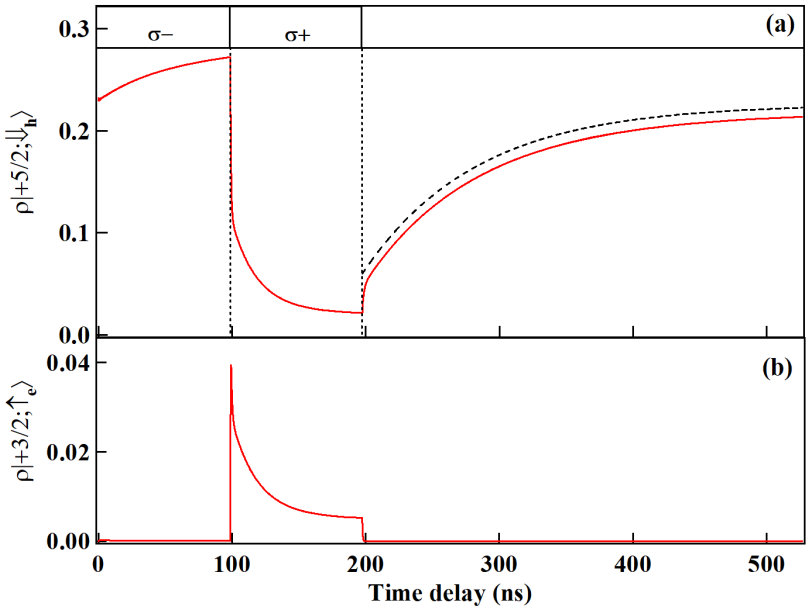

Figure I.14: (a) Calculated time evolution in the dark of the population of the hole-Mn state $|+\frac{5}{2}, \Downarrow_h\rangle$ initialized by a sequence of $\sigma-/\sigma+$ resonant excitation of $|3,-2\rangle$ and $|3,+2\rangle$. The dashed black line (shifted for clarity) is an exponential fit with a characteristic time τ_{relax}=85 ns. (b) Corresponding calculated time evolution of the population $|+\frac{3}{2}, \uparrow_e\rangle$. The parameters are those listed in Tab. I.1.

initially prepared by a sequence of $\sigma-/\sigma+$ excitation resonant with $|3;+2\rangle$ (and $|3;-2\rangle$) is presented in Fig. I.14. When the optical excitation is switched off, after an abrupt jump due to the optical recombination of the charge exciton, the ground hole-Mn state $|+5/2, \Downarrow_h\rangle$ is repopulated in a timescale of about 100 ns, much shorter than the Mn spin relaxation time used in the model ($\tau_{Mn} = 5$ μs). This relaxation in the dark is induced by the presence of VBM: in this case, $\mathcal{H}^{ex}_{hMn}$ couples two by two the different hole-Mn levels. This coupling induces a transfer of population between the different hole-Mn levels. The transfer of population becomes irreversible in the presence of dephasing and controls the observed hole-Mn spin relaxation [5].

The particular behaviour observed for a resonant excitation of the electron-Mn states $|3,+1\rangle$ or $|3,-1\rangle$ (weak photon bunching and no optical pumping at zero field, Fig. I.5 (a) and Fig. I.8 (a) respectively) is also qualitatively explained by the model (see Fig. I.15). The $|3,+1\rangle$ and $|3,-1\rangle$ states are degenerated and differ by a change of angular momentum of two. Consequently, they are efficiently mixed by the anisotropic strain term $E(S_x^2 - S_y^2)$ which induces a spin-flip of two of the Mn

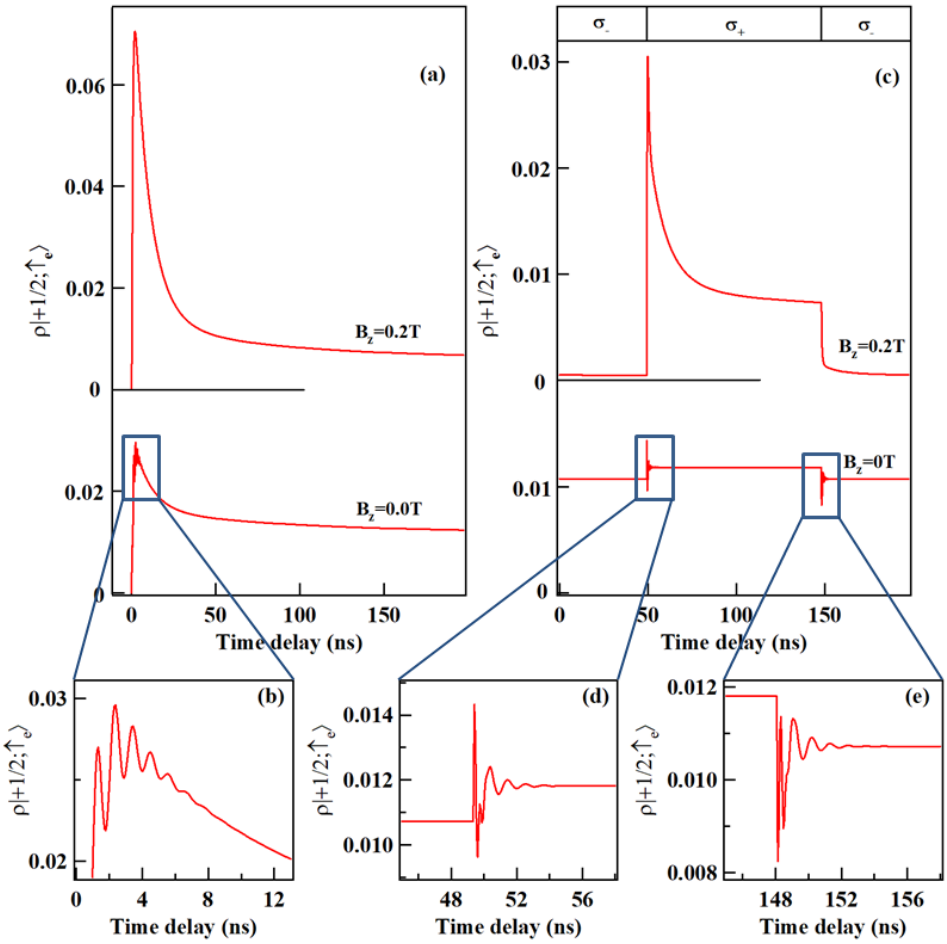

Figure I.15: (a) Calculated time evolution of $\rho_{|+\frac{1}{2},\uparrow_e\rangle}$ with $\rho_{|+\frac{1}{2},\Uparrow_h\rangle}$=1 (hole-Mn spin in the state $|+\frac{1}{2},\Uparrow_h\rangle$ after a $\sigma-$ recombination) for a resonant $\sigma+$ excitation of the coupled electron-Mn states $|3,+1\rangle$ and $|3,-1\rangle$ without and with a longitudinal magnetic field. (b) Zoom on the oscillation appearing in the signal from $|+\frac{1}{2},\uparrow_e\rangle$ at the beginning of a resonant $\sigma+$ excitation. (c) Time evolution of $\rho_{|+\frac{1}{2},\uparrow_e\rangle}$ under excitation with modulated circular polarization. The parameters used in the calculations are those of Fig. I.13. Zoom on the oscillation appearing at the beginning and the end of the $\sigma+$ pusle are presented in, respectively, (d) and (e).

with a conservation of the electron spin. This coupling has no significant influence on the other e-Mn states which are initially split by $D_0 S_z^2$ and $-2\eta S_z^2$.

The splitting between the two new eigenstates, formed by the mixing of $|3,+1\rangle$ and $|3,-1\rangle$, in the μeV range, is much weaker than the width of the resonant laser used in our experiments (around 10 μeV) and the width of the PL lines (around

50 μeV). Under circularly polarized resonant excitation we either excite $|3,+1\rangle$ with $\sigma+$ photons or $|3,-1\rangle$ with $\sigma-$ photons. Under circularly polarized resonant excitation, the two Λ systems associated with $|3,\pm1\rangle$ are simultaneously excited. For alternated circular polarization, a steady state is reached and no pumping transient induced by a leak outside the Λ systems is expected. Under a weak longitudinal magnetic field the Mn Zeeman energy dominates the strain anisotropy term and the coherent transfer is blocked. The states $|3,+1\rangle$ and $|3,-1\rangle$ are decoupled and a large amplitude of bunching and an efficient optical pumping are restored. This behaviour observed in the experiments is qualitatively reproduced by the model.

Let us finally note that in the modelling of optical pumping at zero magnetic field presented in Fig. I.15 (b), fast oscillations are obtained in the first nanoseconds after the polarization switching. These are due to the population transfer between $|3,+1\rangle$ and $|3,-1\rangle$ (directly coupled by E) during the coherence time. These oscillations are too fast to be observed in the experiments. The calculated resonant PL intensity in $\sigma-$ polarization (proportional to $\rho_{|+\frac{1}{2},\uparrow_e\rangle}$) is also slightly larger for a $\sigma+$ excitation than for a $\sigma-$ excitation. The $\sigma-$ resonant PL probes the population of $|3,+1\rangle$ which is directly excited by a resonant $\sigma+$ laser (see the excitation/detection configuration in the inset of Fig. I.8 (a)). On the other hand, under a $\sigma-$ laser, one excites $|3,-1\rangle$ and the charged exciton has a probability to recombine before being transferred to $|3,+1\rangle$ and detected in $\sigma-$ PL. This transfer time results in a slight difference in the steady state resonant PL intensity obtained in a σ_{Co} or σ_{Cross} configuration (see Fig. I.8 (a)).

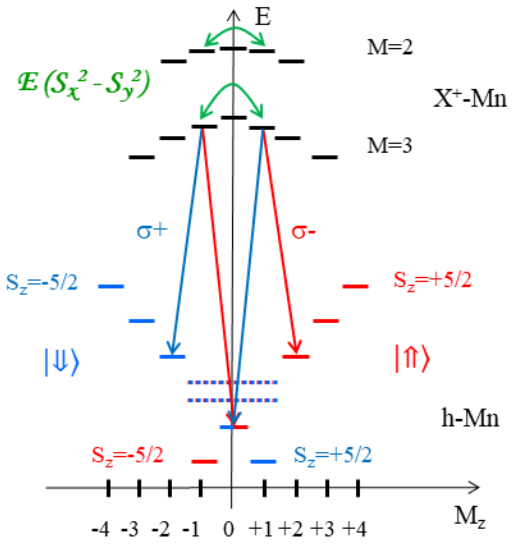

Figure I.16: Copy of Fig. I.3 with a highlight on the coupling induced by the strain anisotropy $E(S_x^2 - S_y^2)$. Optical Λ systems associated with $|3,+1\rangle$ and $|3,-1\rangle$ are presented.

We saw in those last paragraphs that the strain anisotropy is important to understand the dynamic of the e-Mn states $|3, \pm 1\rangle$. Its effect on them is illustrated in Fig. I.16. It prevents the system to be pumped on those states in the absence of longitudinal magnetic field. This beating between the states $|3, +1\rangle$ and $|3, -1\rangle$ can be used to extract the value of the QD strain anisotropy.

I.3 Strain induced coherent dynamics of coupled carriers and Mn spins in a quantum dot

We exploited the Λ-level structure evidenced in Sec. I.1.2 to analyze the coherent dynamics of the e-Mn spin through the time evolution of the circular polarization rate, $\kappa = (\sigma_{Cross} - \sigma_{Co})/(\sigma_{Cross} + \sigma_{Co})$, of the resonant PL. The configuration of the experiment is summarized in Fig. I.17 (a). Circularly polarized and spectrally filtered 10 ps laser pulses are successively tuned on resonance with the high energy lines of the Λ-system associated with the the e-Mn states $|3, +1\rangle$, $|3, +2\rangle$ and $|2, +2\rangle$. We detected with a fast avalanche photodiode with a time resolution of about 60 ps. The QD is excited with sequences of $\sigma+/\sigma-$ pulses (Fig. I.17 (b)), to avoid any possible optical spin pumping of h-Mn [5] that could influence the observed dynamics.

The main result is the observation of an oscillatory behaviour of the polarization rate of the PL when probing the dynamics of the $|3, +1\rangle$ state. The period of the beats is 270 ps with a characteristic damping time of 0.6 ns. When probing the dynamics of the $|3, +2\rangle$ and $|2, +2\rangle$ states, we measured cross circularly polarized PL with a slow decrease of the polarization rate during the lifetime of X^+-Mn.

The origin of this dynamics lies in the mixing of the $|3, +1\rangle$ and $|3, -1\rangle$ states by the anisotropy of strain, as presented in Sec. I.2.3. When a pulsed laser is tuned to the high energy transition of the Λ system associated to $|3, +1\rangle = \frac{1}{\sqrt{6}}(\sqrt{4}|+1/2, \uparrow_e\rangle + \sqrt{2}|+3/2, \downarrow_e\rangle)$ ($\sigma+$ absorption from the h-Mn state $|+3/2, \Downarrow_h\rangle$), the PL of the low energy transition of the Λ system is first cross-circularly polarized ($\sigma-$ recombination to the h-Mn state $|+1/2, \Uparrow_h\rangle$). Then, after a coherent transfer of population to the e-Mn state $|3, -1\rangle = \frac{1}{\sqrt{6}}(\sqrt{2}|-3/2, \uparrow_e\rangle + \sqrt{4}|-1/2\ \downarrow_e\rangle)$ induced by E (Fig.I.17 (c)), co-circularly polarized PL is emitted at the same energy from the $|3, -1\rangle$ state ($\sigma+$ recombination to $|-1/2\rangle|\ \Downarrow\rangle$). This coherent transfer of population is fully controlled by the in-plane anisotropy of the strain at the Mn location and is responsible for the observed oscillations of the circular polarization rate.

To understand the details of this dynamics, we calculated the time evolution of the populations and coherence of the twelve X^+-Mn states and the twelve hole-Mn states. We neglected here the hyperfine coupling between the electronic and

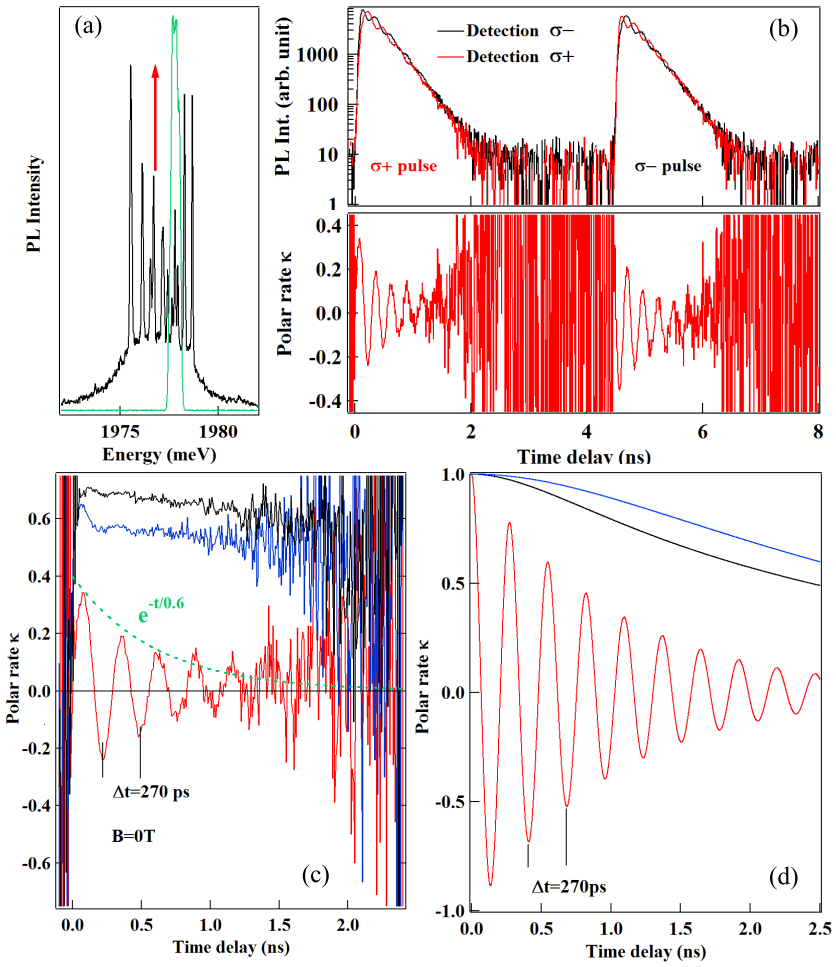

Figure I.17: (a) Configuration of the time resolved PL experiment for an excitation of $|3,+1\rangle$ (pulsed laser in green). (b) Top panel: Time resolved resonant PL of $|3,+1\rangle$ with a $\sigma+/\sigma-$ sequence of laser pulses and a detection in $\sigma+$ and $\sigma-$ polarization. Bottom panel: corresponding time dependence of the circular polarization rate $\kappa = (\sigma_- - \sigma_+)/(\sigma_- + \sigma_+)$. (c) Time dependence of the circular polarization rate of the resonant PL of the states $|3,+1\rangle$ (red), $|3,+2\rangle$ (black) and $|2,+2\rangle$ (blue). (d) Corresponding polarisation rates calculated with $D_0 = 7\mu eV$ [5], $T_2^{eMn} = 0.6ns$, $E = 1.8\mu eV$, a radiative lifetime $T_r = 0.3ns$, $I_{eMn} = -175$ μeV, $I_{hMn} = 345$ μeV., $\frac{\rho_s}{\Delta_{lh}=0.09}$, $\eta = 30$ μeV, $T_{eff} = 20$ K.

nuclear spins of the Mn and solved the master equation for the 24×24 density matrix numerically, including relaxation and pure dephasing processes in the Lindblad form, as presented in Sec. I.2.3.

For the initial condition in the calculation of the time evolution, we consider that a $\sigma+$ pulse on resonance with the high energy side of the Λ-level system (1) (see Fig. I.4) projects the system on the $M = 3$ electron-Mn subspace on all the levels that contain a component $|+3/2, \downarrow_e\rangle$. In the absence of transverse magnetic field and strain anisotropy term E, this excitation simply corresponds to an optical transition from the hole-Mn state $|+3/2, \Downarrow_h\rangle$ towards the electron-Mn state $|3, +1\rangle$. With a weak transverse magnetic field (typically lower than 0.5 T), a linear combination of the $M = 3$ states is created. At large transverse magnetic field, one should consider possible mixing with the $M = 2$ states. Similarly, a $\sigma+$ pulse on (2) projects the system on the $M = 3$ electron-Mn subspace on the levels that contain a component $|+5/2, \downarrow_e\rangle$ and a $\sigma+$ pulse resonant on (3) projects the system on the $M = 2$ electron-Mn subspace on the levels that contain a component $|+5/2, \downarrow_e\rangle$.

After this excitation, the circular polarization of the resonant photoluminescence is governed by the evolution of the spin of the electron. For instance, to compute the circular polarization rate of the emission after a resonant $\sigma+$ excitation on (1) (optical excitation from the hole-Mn state $|+3/2, \Downarrow_h\rangle$ to $|3, +1\rangle$: high energy branch of the Λ-system) we calculate the difference between the density matrix elements $\rho_{|+1/2,\uparrow_e\rangle}$ ($\sigma-$ recombination towards the hole-Mn state $|+1/2, \Uparrow_h\rangle$: low energy branch of the Λ-system) and $\rho_{|-1/2,\downarrow_e\rangle}$ ($\sigma+$ recombination towards the hole-Mn state $|-1/2, \Downarrow_h\rangle$: low energy branch of the Λ-system associated with $|3, -1\rangle$).

In the absence of magnetic field, the period of the quantum beats observed for an excitation of $|3, +1\rangle$ depends only on the anisotropy term E. The experimental data can be well reproduced by the model with $E = 1.8$ μeV (Fig.I.17 (d)). A coherence time, $T_2^{eMn} \approx 0.6$ ns, of the spin of e-Mn is extracted from the damping of the oscillations. For an excitation of $|3, +2\rangle$ and $|2, +2\rangle$ one can observe a slow decrease of the polarization rate which is also qualitatively reproduced by the model.

The coherent transfer of population depends both on the initial splitting of the e-Mn spin states (controlled at zero field by D_0 and η) and on the strength of the coupling E. The splitting between the e-Mn states can be tuned by a magnetic field, B_z, applied along the growth axis. In addition, a coupling between the e-Mn spin states M_z can be induced by a magnetic field, B_x, applied in the QD plane. The experimental and calculated evolution of the polarization rate of the e-Mn states, $|3, +1\rangle$, $|3, +2\rangle$ and $|2, +2\rangle$, versus magnetic field are presented in Fig. I.18.

Under a longitudinal magnetic field B_z, the e-Mn states $M_z = \pm 1$ are split and the influence of E is progressively reduced. For an excitation on the $|3, +1\rangle$ state, the amplitude and period of the oscillations in the polarization rate reduce as B_z increases: the resonant PL becomes cross-circularly polarized with a polarization

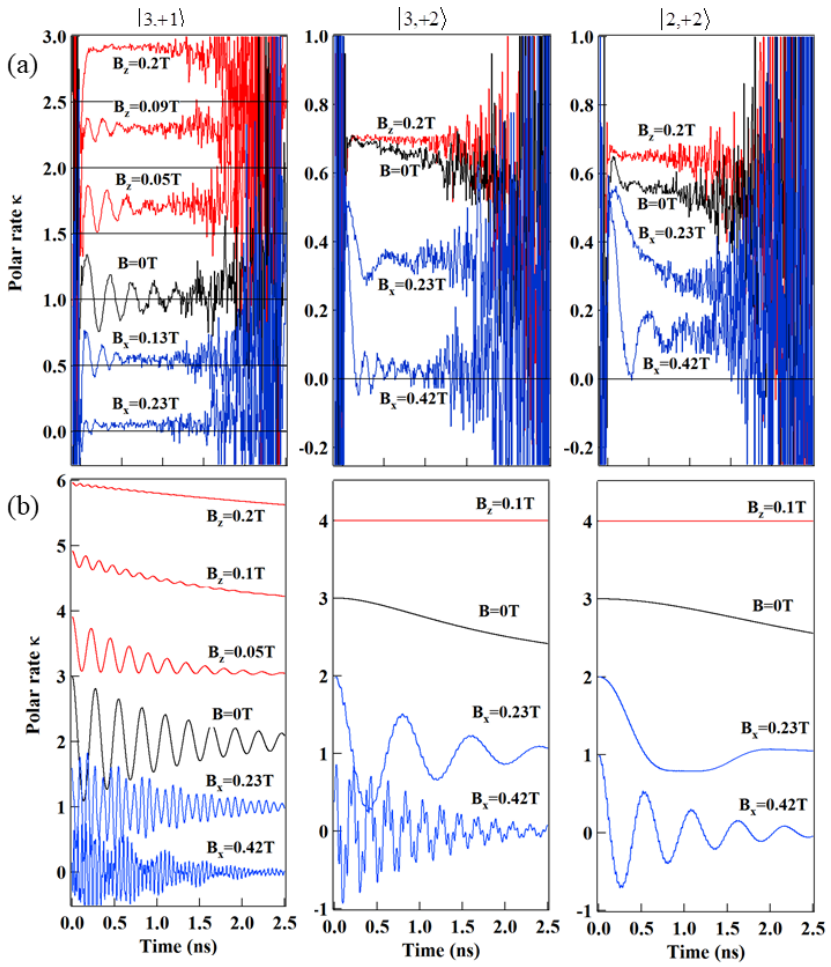

Figure I.18: (a) Influence of a longitudinal (B_z, red) and a transverse (B_x, blue) magnetic field on the time dependence of the circular polarization rate $\kappa = (\sigma_- - \sigma_+)/(\sigma_- + \sigma_+)$ of the resonant PL of $|3,+1\rangle$, $|3,+2\rangle$ and $|2,+2\rangle$. On the top left panel, curves are shifted by 0.5 for clarity. (b) Corresponding time dependence of the circular polarization rate calculated with $g_{Mn} = 2$, $g_e = -0.4$, $g_h = 0.6$ [5], and the parameters of Fig. I.17. The curves are shifted by 1 for clarity.

rate constant during the lifetime of X^+. A weak longitudinal magnetic field stabilizes the spin of the e-Mn states $|3,+2\rangle$ and $|2,+2\rangle$ and their polarization rate remains constant during the lifetime of X^+-Mn.

In a transverse magnetic field B_x, the quantum beats observed for an excitation of $|3,+1\rangle$ are accelerated and the measured circular polarization rate drops to zero as the period of the oscillations becomes smaller than the time resolution of the experimental setup. A given transverse magnetic field induces a slower oscillation

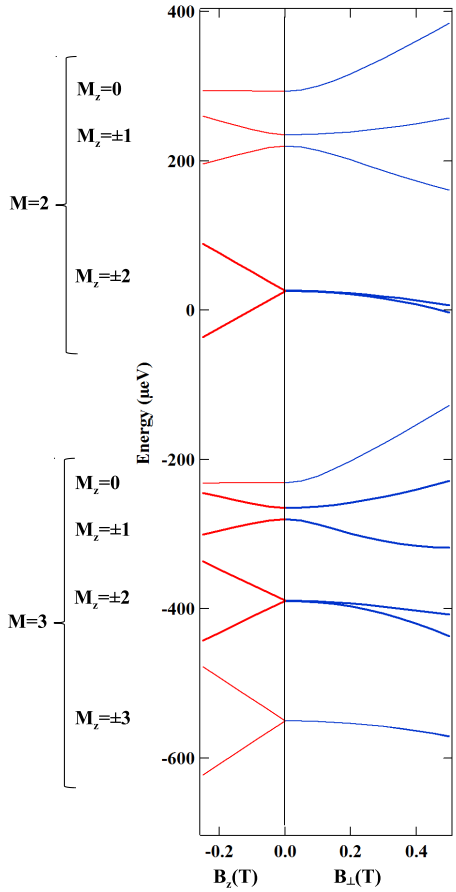

Figure I.19: (Color line) Calculated energy of the electron-M states in a longitudinal magnetic field (B_z) and in a transverse magnetic field ($B_\perp$). The parameters used in the calculations are listed in Fig. I.18.

of the polarization rate for the states $|3,+2\rangle$ and $|2,+2\rangle$.

The observed magnetic field dependence of the coherent dynamics of $|3,+1\rangle$, $|3,+2\rangle$ and $|2,+2\rangle$ can be qualitatively reproduced by the model with the exchange parameters deduced from the PL and the strain anisotropy term and coherence time deduced from the oscillations observed on $|3,+1\rangle$ at zero magnetic field (Fig.I.17). D_0 cannot be extracted from these measurements and we use a typical value $D_0 = 7$ μeV corresponding to a partial relaxation of the biaxial strain [5]. The different precession periods observed for the three states in a given transverse magnetic field are particularly well described.

The evolution of the coherent dynamic under magnetic field is a consequence of the magnetic field dependence of the energy, illustrated on Fig. I.19. In a longitudinal magnetic field, the electron-Mn states $M_z = \pm$i are split by the Mn Zeeman energy, stabilizing their spin states. The degeneracy of the levels with an angular momentum $M_z = \pm 1$ is lifted and the small E value is not enough to

couple them. Therefore, the oscillations observed in the polarization disappear for a high enough magnetic field.

In a transverse magnetic field, the observed splitting of the states $M_z = \pm$i strongly depend on the considered levels. The field induced splitting results in this case from mixing of electron-Mn states with a difference in total angular momentum $\Delta M_z = \pm 1$. These states are initially irregularly separated at zero field resulting in different transverse magnetic field induced coupling.

Conclusion

We studied in this chapter the details of the energy structure and the dynamics of the coupled carriers and Mn spins in a positively charged quantum dot. We saw that the ground state consists of hole-Mn hybrid spin states, and the excited state is dominated by the e-Mn interaction. This leads to an ensemble of optical Λ-level systems. This opens the possibility to perform a coherent manipulation of the magnet formed by the coupled h-Mn spins with two resonant optical fields [23]. We used these systems to study the spin resonant dynamics of positively charged Mn-doped CdTe/ZnTe QD.

Using those, we identified and efficient spin relaxation channel for the hybrid hole-Mn spin in a QD. We propose these hole-Mn flips-flops to be caused by the interplay of the exchange interaction and the lattice deformation of acoustic phonons. The characteristic time of these flip-flops depends on the splitting between the two considered hole-Mn states, and are found in our Λ-system to be of the nanosecond time scale. This reproduce well the experiments and shows that these flip-flops are responsible for the large PL intensity observed under resonant excitation of of the Λ-systems. Jumps out of these systems are possible and induce a large bunching in the resonant PL. They also are at the origin of the optical hole-Mn spin observed under circularly polarized resonant excitation. We can enhance the escape out of the excited Λ system by applying a transverse magnetic field, mixing the e-Mn states in the excited state of the charged QD. This fast h-Mn dynamic dynamics makes this hybrid spin not ideal for practical use for quantum information device. However, the use of a different QD systems with a better hole confinement and a larger hh-lh splitting could significantly reduce the influence of valence band mixing on the hole-Mn spin relaxation and limit the interaction of the hybrid spin with acoustic phonons.

Another interesting point was found for Mn in positively charged strained quantum dots probing the time dependence of the resonant PL polarization for each Λ-level system. We saw oscillations in the one associated with the excited state $|3, +1\rangle$ when a stable polarization of the emission was expected. We explained this by a control of the electron and Mn spins coherent dynamics by the strains ampli-

tude and symmetry at the Mn location. These results demonstrate the potential of magnetic QDs where one could exploit the intrinsic spin(strain interaction to coherently couple the spin of a magnetic atom to the motion of a nano-mechanical oscillator [26, 27] and suggest some possible coherent mechanical spin-driving of a magnetic atom.

Coupling spins to a mechanical oscillator open new way to manipulate spin. In the next chapter, we will study a system with a non-zero orbital momentum, and thus more strongly coupled to the strain state than the Mn atom: a single Cr atom in a II-VI quantum dot.

Bibliography

[1]K. Výborný, J. E. Han, R. Oszwałdowski, I. Žuti ć, and A. G. Petukhov, "Magnetic anisotropies of quantum dots doped with magnetic ions", Phys. Rev. B **85**, 155312 (2012).

[2]L. Besombes, H. Boukari, C. L. Gall, B. Brunetti, C. Cao, S. Jamet, and B. Varghese, "Optical control of the spin of a magnetic atom in a semiconductor quantum dot", Nanophotonics **4**, 75 (2015).

[3]J. Fernández-Rossier, "Single-exciton spectroscopy of semimagnetic quantum dots", Phys. Rev. B **73**, 045301 (2006).

[4]Y. Léger, L. Besombes, L. Maingault, and H. Mariette, "Valence-band mixing in neutral, charged, and Mn-doped self-assembled quantum dots", Phys. Rev. B **76**, 045331 (2007).

[5]B. Varghese, H. Boukari, and L. Besombes, "Dynamics of a Mn spin coupled to a single hole confined in a quantum dot", Phys. Rev. B **90**, 115307 (2014).

[6]L. Besombes, Y. Leger, L. Maingault, D. Ferrand, H. Mariette, and J. Cibert, "Carrier-induced spin splitting of an individual magnetic atom embedded in a quantum dot", Phys. Rev. B **71**, 161307 (2005).

[7]A. H. Trojnar, M. Korkusinski, U. C. Mendes, M. Goryca, M. Koperski, T. Smolenski, P. Kossacki, P. Wojnar, and P. Hawrylak, "Fine structure of a biexciton in a single quantum dot with a magnetic impurity", Phys. Rev. B **87**, 205311 (2013).

[8]L. Besombes and H. Boukari, "Resonant optical pumping of a Mn spin in a strain-free quantum dot", Phys. Rev. B **89**, 085315 (2014).

[9]L. Besombes, K. Kheng, L. Marsal, and H. Mariette, "Acoustic phonon broadening mechanism in single quantum dot emission", Phys. Rev. B **63**, 155307 (2001).

[10]E. Tsitsishvili, R. v. Baltz, and H. Kalt, "Exciton spin relaxation in single semiconductor quantum dots", Phys. Rev. B **67**, 205330 (2003).

[11]K. Roszak, V. M. Axt, T. Kuhn, and P. Machnikowski, "Exciton spin decay in quantum dots to bright and dark states", Phys. Rev. B **76**, 195324 (2007).

[12]S. Adachi, "Properties of group IV, II-V and II-VI semiconductors", in, edited by Wiley (2005) Chap. 8, p. 178.

[13]G. Mahan, *Many-particle physics*, edited by N. Y. Plenum Press (1993).

[14]L. M. Woods, T. L. Reinecke, and R. Kotlyar, "Hole spin relaxation in quantum dots", Phys. Rev. B **69**, 125330 (2004).

[15]P. Michler, *Single quantum dots fundamentals, applications and new concepts*, edited by B. Springer (2003).

[16]J.-W. Luo, G. Bester, and A. Zunger, "Supercoupling between heavy-hole and light-hole states in nanostructures", Phys. Rev. B **92**, 165301 (2015).

[17]M. P. van Exter, J. Gudat, G. Nienhuis, and D. Bouwmeester, "Spin quantum jumps in a singly charged quantum dot", Phys. Rev. A **80**, 023812 (2009).

[18]C. Roy and S. Hughes, "Influence of electron-acoustic-phonon scattering on intensity power broadening in a coherently driven quantum-dot-cavity system", Phys. Rev. X **1**, 021009 (2011).

[19]S. Jamet, H. Boukari, and L. Besombes, "Spin dynamics of a mn atom in a semiconductor quantum dot under resonant optical excitation", Phys. Rev. B **87**, 245306 (2013).

[20]C. L. Cao, L. Besombes, and J. Fernández-Rossier, "Spin-phonon coupling in single mn-doped cdte quantum dot", Phys. Rev. B **84**, 205305 (2011).

[21]Ł. Cywi ński, "Optical orientation of a single mn spin in a quantum dot: role of carrier spin relaxation", Phys. Rev. B **82**, 075321 (2010).

[22]C. Le Gall, A. Brunetti, H. Boukari, and L. Besombes, "Electron-nuclei spin dynamics in ii-vi semiconductor quantum dots", Phys. Rev. B **85**, 195312 (2012).

[23]J. Houel, J. H. Prechtel, A. V. Kuhlmann, D. Brunner, C. E. Kuklewicz, B. D. Gerardot, N. G. Stoltz, P. M. Petroff, and R. J. Warburton, "High resolution coherent population trapping on a single hole spin in a semiconductor quantum dot", Phys. Rev. Lett. **112**, 107401 (2014).

[24]A. O. Govorov and A. V. Kalameitsev, "Optical properties of a semiconductor quantum dot with a single magnetic impurity: photoinduced spin orientation", Phys. Rev. B **71**, 035338 (2005).

[25]C. Cohen-Tannoudji, B. Diu, and F. Laloe, *Mecanique quantique*, edited by P. Hermann (1973).

[26] S. Kolkowitz, A. C. Bleszynski Jayich, Q. P. Unterreithmeier, S. D. Bennett, P. Rabl, J. G. E. Harris, and M. D. Lukin, "Coherent sensing of a mechanical resonator with a single-spin qubit", Science **335**, 1603–1606 (2012).

[27] J. Teissier, A. Barfuss, P. Appel, E. Neu, and P. Maletinsky, "Strain coupling of a nitrogen-vacancy center spin to a diamond mechanical oscillator", Phys. Rev. Lett. **113**, 020503 (2014).